Molina Puerto, J.; Fernández Sáez, J.; Del Río García, AI.; Bonastre Cano, JA.; Cases, F. (2014). Synthesis of Pt nanoparticles on electrochemically reduced graphene oxide by potentiostatic and alternate current methods. Materials Characterization. 89:56-68. doi:10.1016/j.matchar.2014.01.003.

# Synthesis of Pt nanoparticles on electrochemically reduced graphene oxide by potentiostatic and alternate current methods

J. Molina†, J. Fernández, A.I. del Río, J. Bonastre, F. Cases*

*Departamento de Ingeniería Textil y Papelera, EPS de Alcoy, Universitat Politècnica de València, Plaza Ferrándiz y Carbonell s/n, 03801 Alcoy, Spain*

## Abstract

Reduced graphene oxide (RGO) has been synthesized on Pt wires by means of a potentiodynamic method between +0.6 V and -1.4 V for 20 scans. Cyclic voltammetry characterization of the coatings showed the typical capacitative behavior of graphene. Pt nanoparticles were synthesized on Pt-RGO electrodes by means of potentiostatic methods and a comparison between different synthesis potential (-0.16, 0, +0.2 and +0.4 V) for the same synthesis charge ($mC \cdot cm^{-2}$) was established. The electrodes obtained were characterized in 0.5 M $H_2SO_4$ solution to observe the characteristic oxidation and reduction processes of the Pt surface. A 0.5 M $H_2SO_4$ / 0.5 M $CH_3OH$ solution was used to measure the catalytic properties of the deposits against methanol oxidation. The most appropriate potential to perform the synthesis was 0 V followed by -0.16 V and +0.2 V. The morphology of the coatings varied depending on the potential applied as observed by scanning electron microscopy. Alternate current methods were also used to synthesize Pt nanoparticles and compare the results with the traditional potentiostatic method. Different frequencies were used: 0.1, 1, 10, 100, 1000 and 10000 Hz. Alternate current synthesis is more efficient than traditional potentiostatic methods, obtaining more electroactive coatings with less effective synthesis time.

**Keywords:** reduced graphene oxide, electrochemical reduction, platinum nanoparticles, alternate current methods, potentiostatic methods.

---

* Corresponding author. Fax.: +34 966528438; telephone: +34 966528412. E-mail address: fjcases@txp.upv.es (Prof. F. Cases).

†Present address: Department of Textile Engineering, University of Minho, Campus de Azurém, 4800-058 Guimarães, Portugal.

## 1. Introduction

Graphene and its derivatives have attracted a great deal of attention due to the exciting electronic, mechanical, optical or thermal properties shown by this material [1-8]. These properties have opened a new era in materials science and physics with a range of different applications. The properties of graphene are greatly influenced by the presence of defects in its structure, so the investigation of methods to produce materials with fewer defects is an active area of development [7-9]. The first method of production reported in literature consisted of the mechanical exfoliation of graphene sheets from graphite [1]. Although high quality graphene sheets with low content of defects were obtained, the production by this method was minimal and the sheets obtained could only be used to carry out fundamental studies. This is the reason why other production methods have been developed, methods such as chemical vapor deposition or chemical methods. The chemical methods are of particular interest since larger quantities of graphene derivatives can be obtained. One of these methods is the oxidation of graphite

to graphene oxide. Graphene oxide is electrically insulating but its conductivity can be partially restored by reduction [9]. Traditional chemical methods have been used for this purpose. Chemical reductants used have been hydrazine [9], dimethylhydrazine [9], hydroquinone [9], $NaBH_4$ [9] and dithionite salts [10]. However some of these salts are very toxic [10], meaning that electrochemical methods could be more appropriate since the only reactive employed is the electron, without the need of additional chemical products. The limitations of electrochemical methods are that the electrode or sample where the reduction takes place must be conductive, be electrochemically active and be in contact with the solution. In literature, the electrochemical reduction of graphene oxide has been performed on different electrode materials such as glassy carbon [11-16], gold [13-17], indium tin oxide (ITO) [12, 14] or Pt [15, 16].

Graphene has also attracted attention due to its very high specific surface area (2630 $m^2 \cdot g^{-1}$) [9]. This high surface area makes graphene very interesting to disperse Pt nanoparticles in order to enhance the electroactivity of electrodes for using them in methanol oxidation in fuel cells [18-27], counter electrodes for dye sensitized solar cells [28, 29], hydrogen gas sensing [30], oxalic acid sensing [31], DNA detection [32], etc. Other metals and alloys have been also deposited on graphene taking advantage of its high specific surface area, such as Pt-Ru [33], Pd [34] or Zn [35]. The methods employed for the synthesis of Pt nanoparticles on graphene have been mainly chemical. Electrochemical methods have been used in less extension. In this work, alternate current was generated with electrochemical impedance spectroscopy equipment. This procedure has not been reported in literature to the best of our knowledge for the synthesis of Pt nanoparticles on graphene coated electrodes. A previous paper suggested that this technique could be used for the synthesis of Pt nanoparticles on conducting polymers [36]. However, the wide frequency range (100 KHz/ 0.1 Hz for example) used

by the authors meant that they could not draw any conclusions about which frequencies could be better for the synthesis of Pt nanoparticles. In addition, the potential employed by the authors could not be the most appropriate (-0.16 V vs. Ag/AgCl (3.5 M KCl) reference electrode), as Pt deposition starts at higher potentials. We should take into account that EIS equipment has a measuring time (where the perturbation potential is applied around the fixed potential) but it has also a processing time (where the data is analyzed and the potential remains fixed). If Pt synthesis happens at the fixed potential, contributions to the synthesis can be expected from alternate current methods but also from the fixed potential (direct current); it would be like a potentiostatic deposition with little potential variation during the alternate current method. In this paper different narrow frequency ranges have been evaluated: [0.1-0.08] Hz, [1-0.8] Hz, [10-8] Hz, [100-80], [1000-800] and [10000-8000] Hz. In addition, the fixed potential has been carefully selected at a potential where Pt deposition does not happen (+0.4 V vs. Ag/AgCl (3.5 M). In this way, the only contribution expected to the synthesis of Pt nanoparticles is the alternate current (ac) applied. To achieve the most appropriate synthesis potential, an amplitude perturbation of ±350 mV was applied.

## 2. Experimental

### 2.1. Reagents and materials.

All reagents used were of analytical grade. Monolayer graphene oxide (GO) powders were acquired from Nanoinnova Technologies S.L. (Spain). $LiClO_4$ (lithium perchlorate), $H_2SO_4$ (sulphuric acid), $CH_3OH$ (methanol) and $H_2PtCl_6 \cdot 6H_2O$ (hexachloroplatinic acid hexahydrate) were purchased from Merck.

Pt wires (0.7 mm diameter, 99.99 % purity) were acquired from Engelhard-Clal. The effective length of the electrodes employed (where reaction occurred) was 2 cm (total area 0.44 $cm^2$). The area of the electrodes was controlled with Teflon®. When needed, solutions were deoxygenated by bubbling nitrogen ($N_2$ premier X50S). Ultrapure water was obtained from an Elix 3 Millipore-Milli-Q Advantage A10 system with a resistivity near to 18.2 MΩ·cm.

2.2. Electrochemical synthesis of reduced graphene oxide on Pt.

All electrochemical experiments were performed at room temperature with an Eco-Chemie Autolab PGSTAT302 potentiostat/galvanostat. Electrochemical synthesis of reduced graphene oxide (RGO) on Pt surface was accomplished by the potentiodynamic method. A three-electrode configuration was used with an Ag/AgCl reference electrode, a Pt counter electrode wire and a Pt working electrode wire. The preparation of Pt electrodes consisted of a flame treatment to clean its surface prior to carrying out the synthesis, according to the method developed by Clavilier [37]. The solution used consisted of a 3 $g \cdot L^{-1}$ GO solution in 0.1 M $LiClO_4$. The synthesis with cyclic voltammetry (CV) was performed employing different potential ranges: (+0.6 V↔-0.8 V); (+0.6 V↔-1.0 V); (+0.6 V↔-1.2 V) and (+0.6 V↔-1.4 V) (vs. Ag/AgCl 3.5 M KCl). The number of scans employed to perform the synthesis was 20 and the scan rate was 50 $mV \cdot s^{-1}$. The GO suspension tended to precipitate slowly, reason why bubbling for 3 seconds with $N_2$ gas was applied after the $10^{th}$ scan. After the synthesis, the obtained electrodes were rinsed with water and characterized in 0.1 M $LiClO_4$ aqueous solution to observe the characteristic electrochemical behaviour of RGO. The configuration used was the same as in the synthesis. The highest electrochemical response was obtained for the electrode synthesized with the (+0.6 V↔-1.4 V) potential

range, reason why this range was selected as the optimum one to perform the synthesis of RGO on Pt.

The optimum electrode obtained was also characterized by means of cyclic voltammetry in 0.5 M $H_2SO_4$ solution and compared with the response of Pt. This is the medium employed to characterize the electroactivity of dispersed Pt coated electrodes and it is important to have the electrochemical response of the Pt-RGO electrode in this medium. The potential range used was +0.7 V↔-0.2 V (vs. Ag/AgCl 3.5 M KCl) and the scan rate was 50 $mV \cdot s^{-1}$.

2.3. Electrochemical synthesis of Pt by potentiostatic method on Pt-RGO.

The electrochemical synthesis of Pt on Pt-RGO was accomplished firstly by the potentiostatic method to determine the best potential to carry out the synthesis by alternate current method. A three-electrode configuration was also used; the reference electrode used was Ag/AgCl (KCl 3.5 M), a Pt wire was used as counter electrode and the working electrode was Pt-RGO. The synthesis solution was 5 mM $H_2PtCl_6$ in 0.5 M $H_2SO_4$. Prior to carrying out the potentiostatic synthesis at different potentials, a voltammogram in the synthesis solution was obtained on a Pt-RGO electrode to observe the potential where Pt reduction takes place on RGO surface. A Pt-RGO electrode was also characterized in the blank solution ($H_2SO_4$) to discard redox processes of the RGO surface. Taking into account the voltammograms obtained, different potentials were selected to carry out the potentiostatic synthesis (-0.16 V, 0 V, +0.2 V and +0.4 V) (vs. Ag/AgCl 3.5 M KCl) (Table 1). Potentiostatic synthesis at these potentials was performed with the same synthesis charge (~260 $mC \cdot cm^{-2}$) to compare the results under the same synthesis conditions. The electrodes obtained were characterized in 0.5 M $H_2SO_4$ solution to observe the characteristic oxidation and reduction processes of Pt

nanoparticles surfaces. A 0.5 M $H_2SO_4$ / 0.5 M $CH_3OH$ solution was used to measure the electrocatalytic properties of the deposits for methanol oxidation.

2.4. Electrochemical synthesis of Pt by alternate current methods on Pt-RGO.

The synthesis of Pt was also performed on Pt-RGO with alternate current methods obtained from electrochemical impedance spectroscopy (EIS) equipment. The configuration and materials used were the same as in the potentiostatic method. Different frequency ranges were used to observe the influence of this parameter in the synthesis of Pt nanoparticles on Pt-RGO electrodes. Table 2 shows all the parameters employed for the synthesis of the different samples as well as the nomenclature employed.

The number of points was changed to vary the synthesis time. Although theoretically 20000 points could be obtained with the equipment, problems were encountered when using a number of points higher than 1000. With such high number of points, the frequency was not adequately applied, this is why 1000 points was the maximum value used. The potential from which the measurement started was a potential were Pt synthesis was negligible, this is why +0.4 V (vs. Ag/AgCl 3.5 M KCl) was employed. The applied amplitude was ±350 mV (maximum allowed), so the potential range during the alternate current synthesis varied from +0.05 V to +0.75 V. The synthesis of Pt only took place from +0.4 V to +0.05 V according to the voltammograms of synthesis obtained. This is why the real synthesis time is half the total synthesis time used. For comparison, two samples were also obtained using the entire frequency range (100000 Hz-0.01 Hz) with ±10 mV (negligible Pt synthesis) and ±350 mV (synthesis of Pt takes place) amplitude perturbations. The electroactivity of the electrodes was also measured in 0.5 M $H_2SO_4$ and in 0.5 M $H_2SO_4$ / 0.5 M $CH_3OH$ solutions.

2.5. Field emission scanning electron microscopy (FESEM)

A Zeiss Ultra 55 FESEM (field emission scanning electron microscope) was used to observe the morphology of the samples using an acceleration voltage of 3 kV.

2.6. X-ray photoelectron spectroscopy measurements (XPS)

XPS analyses were conducted at a base pressure of $5\times10^{-10}$ mbars and a temperature of around −100 ◦C. XPS spectra were obtained with a VG-Microtech Multilab electron spectrometer by using unmonochromatized Mg Kα (1253.6 eV) radiation from a twin anode source operating at 300 W (20 mA, 15 kV). The binding energy (BE) scale was calibrated with reference to the C 1s line at 284.6 eV. C 1s, O 1s and Pt4f core levels XPS spectra were analyzed. The sensitivity factors employed were 1 for C1s, 2.93 for O1s, 8.65 for Pt $4f_{7/2}$ and 6.81 for Pt $4f_{5/2}$. The pass energies were, charge compensation, software, area analyzed.

## 3. Results and discussion

3.1. Electrochemical synthesis of reduced graphene oxide on Pt.

Fig. S1-a shows the voltammograms obtained using a Pt working electrode in 0.1 M $LiClO_4$ and 0.1 M $LiClO_4$ / 3 $g{\cdot}L^{-1}$ GO solutions between +0.6 V and -0.8 V (vs. Ag/AgCl 3.5 M KCl). The scan rate employed was 50 mV·s-1. As can be seen, the presence of GO causes the appearance of a redox pair located at -0.34 V and -0.44 V (vs. Ag/AgCl 3.5 M KCl). The presence of this redox pair has been attributed to a highly characteristic chemically reversible $H^+/H_2$ process [16, 38]. We have to take into account that GO has different groups such as carboxylic acids that can release $H^+$ into

the solution. This is why the pH of the GO solution was around 3.6. When the lower potential limit was decreased to -1.4 V (vs. Ag/AgCl 3.5 M KCl), the hydrogen evolution reaction appeared for potentials lower than -0.9 V (Fig. S1-b). Comparing the blank solution (0.1 M $LiClO_4$) and the solution containing GO, it can be seen that the maximum current density reached in the latter case is higher than in the former one (-12.9 $mA \cdot cm^{-2}$ vs. -16.6 $mA \cdot cm^{-2}$). This difference between them can be attributed to the reduction of GO to RGO on the Pt surface. Different lower potential limits for the potentiodynamic synthesis were evaluated (-0.8, -1.0, -1.2 and -1.4 V) (vs. Ag/AgCl 3.5 M KCl). Fig. S2 shows the voltammetric characterization of Pt and RGO-Pt electrodes in 0.1 M $LiClO_4$ aqueous solutions, the scan rate employed was 50 $mV \cdot s^{-1}$. The RGO-Pt electrodes were synthesized by cyclic voltammetry during 20 scans employing different potential ranges: (+0.6 V↔-0.8 V); (+0.6 V↔-1.0 V); (+0.6 V↔-1.2 V) and (+0.6 V↔-1.4 V) (vs. Ag/AgCl 3.5 M KCl). As can be seen in the voltammograms of characterization of Fig. S2, the highest current densities and electrical charge obtained correspond to the synthesis performed with the potential range (0.6 V↔-1.4 V). This is why; this potential range was selected as the best one to perform the synthesis of RGO on Pt electrodes. The bare Pt electrode was also characterized in this solution as reference.

Fig. S3 shows the evolution of the synthesis of RGO on the Pt electrode between +0.6 V and -1.4 V for 20 scans. As can be seen in Fig. S3-a, the hydrogen evolution reaction intensity decreases with the increasing number of scans. Also the $H^+/H_2$ redox pair (Fig. S3-b) decreases its intensity and becomes more irreversible. This variation in the redox processes can be attributed to the synthesis of RGO on the Pt surface [16]. The color of the RGO coating on Pt was blackish, indicating the reduction of graphene oxide [8].

The optimum electrode synthesized employing the (+0.6 V↔-1.4 V) potential range and bare Pt electrode were also characterized in 0.5 M $H_2SO_4$ medium, which is the medium employed to test the electroactivity of dispersed Pt coatings (Fig. 1). In the case of the Pt electrode, the characteristic oxidation and reduction processes of the Pt surface could be observed at potentials lower than +0.1 V and higher than +0.5 V (vs. Ag/AgCl 3.5 M KCl) [39-42]. It could be seen that when RGO was deposited on Pt for 20 scans between +0.6 V and -1.4 V, the presence of these redox peaks was clearly diminished. Some residual activity was still present, due to the availability of Pt sites as XPS measurements have shown. Instead of this, the appearance of the characteristic capacitative behaviour of graphene was evident [17]. This confirmed the formation of RGO on the surface of the Pt electrodes. Evidence of the formation of RGO coating was also obtained from scanning electron microscopy. Fig. 2 shows the micrographs of a Pt electrode coated with RGO. As can be seen in Fig. 2-a, the electrode is completely coated with RGO. Reduced graphene oxide sheets can also be observed with higher magnification as shown in Fig. 2-b. The typical wrinkles of graphene sheets help to locate them [43].

X-ray photoelectron spectroscopy was used to characterize chemically the samples coated with RGO. Fig. S4 shows the survey spectra of the Pt-RGO electrode. Fig. 3 shows the high resolution C 1s and O 1s XPS spectrum for the RGO sample. The atomic percentage of C and O was 82.46 and 12.05 %, respectively. Pt was also analyzed, obtaining an atomic content of 5.49 %. The Pt4f XPS spectrum is also shown in Fig. S5. This low percentage of Pt would indicate that some portion of Pt surface was not coated with RGO. Four peaks were deconvoluted in Pt4f spectrum. The two peaks at 71.2 eV ($Pt4f_{7/2}$) and 74.4 eV ($Pt4f_{5/2}$) were assigned to a spin-orbit coupling doublet. The doublet separation of 3.2 eV is characteristic of platinum element (Pt4f) [44]. These

binding energies were due to metallic Pt [45]. The other doublet obtained at 72.3 eV ($Pt4f_{7/2}$) and 75.2 eV ($Pt4f_{5/2}$) was assigned to Pt ionic species [44] probably due to surface Pt oxides. The analysis of the C 1s core level spectra is shown in Fig. 3-a, three peaks were deconvoluted at 284.5, 285.7 and 286.9 eV. The first peak at 284.5 eV was attributed to $sp^2$ carbon in the graphitic network. The peak at 285.7 eV was due to C-OH groups. The peak at 286.9 eV was ascribed to C=O and C-O-C (epoxy $sp^3$ carbon bonds on the basal plane) groups [46]. The $sp^2$ fraction (obtained dividing the $sp^2$ carbon content by the total carbon content) was 0.7. The analysis of the O 1s high resolution XPS spectrum for RGO sample showed two peaks at 531.5 and 532.9 eV (Fig. 3-b). The first peak was ascribed to O=C groups and the second peak was attributed to O-C groups [47]. The O 1s/C 1s ratio gives an indication of the oxygen content and the value obtained for the RGO sample was 0.15. In our previous paper [48], this ratio was around 0.20-0.26 for RGO samples obtained by chemical reduction with sodium dithionite. Therefore, minor oxygen content was obtained by means of the electrochemical reduction compared to the chemical reduction.

3.2. Electrochemical synthesis of Pt by potentiostatic methods on Pt-RGO.

Fig. 4 shows the voltammograms of RGO-Pt electrodes (previously obtained after 20 scans of synthesis between +0.6 V and -1.4 V) in 0.5 M $H_2SO_4$ and in 0.5 M $H_2SO_4$ / 5 mM $H_2PtCl_6$ solutions. The voltammogram performed in the solution containing $H_2PtCl_6$ shows different features that can be attributed to the reduction of Pt on the surface of RGO. Although the maximum of the peak was obtained at -0.16 V, the reduction of Pt species began at potentials lower than + 0.4 V as can be seen in the voltammograms.

The reactions that take place during the reduction of $H_2PtCl_6$ to Pt and the theoretical potentials are [49]:

$$PtCl_6^{2-} + 2e^- \longleftrightarrow PtCl_4^{2-} + 2Cl^- \,(0.515 Vvs.Ag/AgCl(3.5M))$$
$$PtCl_4^{2-} + 2e^- \longleftrightarrow Pt + 4Cl^- \,(0.525 Vvs.Ag/AgCl(3.5M))$$

To determine the most adequate synthesis potential of Pt nanoparticles on the RGO surface, different potentials were evaluated; +0.4 V, +0.2 V, 0 V and –0.16 V (vs. Ag/AgCl 3.5 M KCl) (Table 1 The same electrical charge of 260 mC·cm$^{-2}$ was applied for all the samples. The chronoamperometry curves obtained for the different synthesis potentials can be seen in Fig. S6. The Pt content (μg·cm$^{-2}$) can be calculated by means of the synthesis charge (mC·cm$^{-2}$) (data obtained from the potentiostat/galvanostat equipment) assuming that the single process that happens is the reduction of $PtCl_6^{2-}$ to Pt with complete efficiency (100 %) [50, 51]. The quantity of Pt ($m_{Pt}$) was calculated according to Equation 1:

$$m_{Pt} = \frac{Q_{Pt} \cdot M}{4 \cdot F} \qquad \textbf{(1)}$$

Where: $Q_{Pt}$ is the synthesis charge (C·cm$^{-2}$); M is the Pt atomic weight (195.09 g·mol$^{-1}$); 4 is the number of electrons involved in the reduction of $PtCl_6^{2-}$ to Pt and F is the Faraday constant (96485.3 C·mol$^{-1}$). The load of Pt obtained for the synthesis charge of 260 mC·cm$^{-2}$ was approximately 131.4 μg·cm$^{-2}$.

Fig. 5-a shows the voltammetric characterization in 0.5 M $H_2SO_4$ of the different electrodes obtained by potentiostatic synthesis. The hydrogen adsorption charge was calculated by means of the integration of the area [19] in the corresponding voltammogram (Table 1). The hydrogen adsorption charge obtained for the electrodes obtained with the different synthesis potentials followed this order: 0 V > -0.16 V > +0.2 V > 0.4 V. At +0.4 V the synthesis of Pt was negligible since characteristic

oxidation and reduction processes on Pt were not observed. The electrochemical surface area of Pt (ECSA) of the different electrodes was calculated [19]. The roughness factor was also calculated taking into account the hydrogen adsorption charge and the theoretical value for the adsorption of a hydrogen monolayer on Pt surface (210 $\mu C \cdot cm^{-2}$) as an indication of surface area [40]. Values obtained can be observed in Table 1 and followed the same order as hydrogen adsorption charge values. The highest value of ECSA (electrochemical surface area) obtained at 0 V can be correlated to the lower Pt nanoparticle size as was observed by SEM. The lower the particle size, the higher the roughness and the higher the surface area. Consequently, the electroactivity is improved since more Pt area is available for reaction [40, 41].

Another characteristic probe of the electrocatalytic properties of Pt coatings can be obtained from the oxidation of methanol in acidic solutions. Fig. 5-b shows the voltammograms of characterization in 0.5 M $H_2SO_4$ / 0.5 M $CH_3OH$ for the different electrodes obtained. In the voltammograms, two peaks were observed, one in the forward scan located around +0.65 V (vs. Ag/AgCl 3.5 M KCl) and the other in the backward scan at +0.45 V (vs. Ag/AgCl 3.5 M KCl). The first one is produced due to the oxidation of freshly chemisorbed species coming from methanol adsorption. The second oxidation peak is related to the removal of carbonaceous species not completely oxidized in the forward scan [52, 53]. No electrocatalytic properties for the methanol oxidation were observed for the sample synthesized at +0.4 V, confirming that at this potential the synthesis of Pt does not happen in a significant way. Table 1 shows the maximum values of current density obtained for both peaks for the different electrodes synthesized. Results of electroactivity against methanol oxidation can be directly correlated with the higher surface area of the electrodes obtained in this order 0 V > -0.16 V > +0.2 V.

Scanning electron microscopy was also used to observe the morphology of the coatings obtained. Since the same electrical charge was applied to synthesize all the electrodes, the difference in electroactivity is related to the morphology and particle size of the coatings obtained. Fig. 6 shows micrographs of Pt-RGO electrodes coated with Pt nanoparticles using different synthesis potentials. The morphology of the Pt nanoparticles greatly depends on the applied potential. Fig. 6-a shows a micrograph where the synthesis potential used was -0.16 V. The morphology obtained is flower-like nanorods aggregates [54, 55]. When higher magnification was employed (Fig. 6-b) it could be seen that the particles had needle form and they were very sharp and with very low size (less than 50 nm in the base). This type of growth could be attributed to a rapid growth of the coating with the creation of a high number of nucleation points. These nucleation points developed in the first stage grow and form the flower-like structure [55]. As can be seen in the voltammogram, -0.16 V (vs. Ag/AgCl 3.5 M KCl) was selected because it corresponded to the highest current density (~ -2.3 $mA \cdot cm^{-2}$) obtained in the voltammogram of synthesis (Fig. 4). These flower-like structures have shown more electroactivity than traditional spherical nanoparticles because of its high active surface area [54, 55]. Fig. 6-c shows the micrograph of an electrode obtained using the synthesis potential of 0 V (vs. Ag/AgCl 3.5 M KCl). In this case, the coating is constituted by Pt nanoparticles with very low size and very tightly packed. The Pt nanoparticles can be observed better with the higher magnification micrograph (Fig. 6-d), the size of the nanoparticles is around 30-40 nm. In this case the growth is produced in 2-D with a high order and also with a very low nanoparticle size. In the voltammogram of synthesis (Fig. 4) it can be seen that at this potential there was also a noticeable current density (~ -0.9 $mA \cdot cm^{-2}$). Therefore a lot of nucleation points are also created at this potential, obtaining very low size Pt nanoparticles. The lower growth rate

allows the attainment of a more densely packed coating. When GO or RGO are employed, the size of the nanoparticles and its distribution is improved [55]. Fig. 6-e,f show the micrograph of the coating obtained when +0.2 V (vs. Ag/AgCl 3.5 M KCl) was employed as the synthesis potential. In this case, Pt spherical nanoparticles with higher size than the former cases can be observed (around 200 nm). In this case, the growth of Pt nanoparticles at +0.2 V is slower and also the number of nucleation points is less. This allows the growth of these nucleation points so that particles with greater size are obtained. Fig. 4 also shows that the current density obtained was around -0.2 $mA \cdot cm^{-2}$ (substantially lower than at -0.16 V and 0 V). Finally the potential of +0.4 V (vs. Ag/AgCl 3.5 M KCl) was also used to observe whether there was synthesis at this potential. At this potential no substantial growth of Pt nanoparticles was observed. This confirms the suitability of this potential to be employed as starting potential (where the synthesis of Pt nanoparticles does not take place in a significant way) to produce the synthesis of Pt nanoparticles by alternate current methods (section 3.3). The most electroactive coatings were obtained with the synthesis at 0 V followed by -0.16 V and +0.2 V. These results can be correlated with the lower grain size of Pt nanoparticles following the latter order. The lower grain size produces an increase of the Pt surface area and hence an increase of electroactivity [40, 41].

3.3. Electrochemical synthesis of Pt by alternate current methods on Pt-RGO.

EIS technique is based on applying a potential perturbation of certain amplitude (from ±0.2 mV to ±350 mV) around a fixed potential (by us) with varying frequency. As was commented previously, if the potential is fixed in a zone where Pt synthesis happens (E< +0.4 V (vs. Ag/AgCl 3.5 M KCl), as can be seen in Fig. 4), the synthesis of Pt will be taking place all the time, then a mixture of alternating current (ac) and potentiostatic

synthesis would be obtained. This is why the potential of +0.4 V (vs. Ag/AgCl 3.5 M KCl) was fixed as the starting potential since the synthesis of Pt nanoparticles was not observed. From +0.4 V, which was the fixed potential, the potential varied to +0.05 V and +0.75 V (vs. Ag/AgCl 3.5 M KCl) with the amplitude perturbation of ±350 mV (maximum amplitude perturbation that could be applied with the equipment). The synthesis of Pt nanoparticles takes place between +0.05 V and +0.4 V (vs. Ag/AgCl 3.5 M KCl).

Fig. 7 shows the impedance modulus $|Z|$ vs. the frequency (Hz) plot obtained for the different experiments of Pt synthesis on Pt-RGO electrodes using alternate current methods. In Fig. 7-a the data represented by (◊) is the data obtained using the $10^{5}$-$10^{-2}$ Hz frequency range with ±10 mV amplitude perturbation. In these conditions the synthesis of Pt was very low since the potential range obtained (+0.39, +0.41 V) was very close to the potential at which Pt deposition did not happen (+0.4 V). When the amplitude was increased to ±350 mV the potential range obtained was (+0.05 V, +0.75 V) and the synthesis of Pt took place in a significant way (□). This is why the impedance modulus lowered with regard to the sample synthesized using the ± 10 mV amplitude perturbation. This decrease of the impedance modulus can be attributed to the synthesis of Pt that is taking place on the surface of RGO. When the individual frequency ranges of Table 2 were used (represented in Fig. 7 as coloured lines), a decrease in the impedance modulus $|Z|$ was also observed as the synthesis proceeded. In the case of the 10 Hz electrode synthesis, this decrease was more than one order of magnitude. As can be seen in Fig. 7-b the data for the 10 Hz electrode synthesis has been magnified for best observation.

Fig. 8 shows the voltammetric characterization of the different electrodes obtained using the alternate current synthesis method of Pt nanoparticles. Table 2 shows the results of

hydrogen adsorption charge, roughness factor and maximum current densities obtained for methanol oxidation for the different electrodes obtained. The sample obtained by potentiostatic synthesis at +0.4 V (vs. Ag/AgCl 3.5 M KCl) for 6000 s showed no significant electrochemical activity against hydrogen evolution reaction and methanol oxidation. This confirms that the synthesis of Pt nanoparticles did not take place in a significant way at this potential. In order to compare the different synthesis frequency ranges, the same synthesis time (55. 6 s) was used in the samples of 0.1 Hz, 1 Hz and 10 Hz. With the other frequencies, this synthesis time could not be achieved due to the limitation in the number of points that could be recorded. Taking into account the results obtained for hydrogen adsorption charge, roughness factor and maximum current densities for methanol oxidation (Table 1), the most electroactive electrodes followed this order: 10 Hz > 1 Hz > 0.1 Hz. An increase in the synthesis frequency, produced an increase in the electroactivity of the electrodes (Fig. 8-a, Fig. 8-b and Table 2). This indicates that higher frequencies are the most appropriate to perform the synthesis by alternate current methods. If the best results for potentiostatic synthesis (synthesis at 0 V vs. Ag/AgCl 3.5 M KCl) are compared with the best results for alternate current synthesis (10 Hz synthesis), it can be seen that the hydrogen adsorption charge and methanol oxidation current densities values are almost double in the case of the alternate current synthesis than in the potentiostatic synthesis. Conversely, the effective synthesis time is lower in the case of alternate current synthesis at 10 Hz (55.6 s vs. 467 s for the potentiostatic synthesis at 0 V). It can be concluded that alternate current synthesis by EIS can be used effectively to produce more electroactive coatings.

The other frequencies used for the synthesis were not comparable since the same synthesis time was not achieved. However, the results should be reported briefly. In the sample obtained with 100 Hz, the synthesis time was 10 times lower than in the case of

10 Hz. However, the hydrogen adsorption charge obtained was similar to that obtained for 10 Hz. Conversely, the electrocatalytic activity for methanol oxidation was much higher in the case of 10 Hz synthesis. This difference of electroactivity could be attributed to the appearance of cracks on the surface of the coating obtained employing 100 Hz, due to a massive growth of the coating (as observed by SEM). When even higher frequencies such as 1000 and 10000 Hz were employed, significant results were not observed since the synthesis time achieved was very low. Future studies could be carried out with continuous potential pulse generators to study the influence of such high frequencies on the synthesis of Pt nanoparticles.

Another electrode was synthesized using the complete frequency range ($10^5$-$10^{-2}$ Hz). In this case, the electroactivity obtained was similar to the 1 Hz sample. However the effective synthesis time is 3 times lower in the case of 1 Hz frequency, as can be seen in Table 2. This fact points out again the importance of the synthesis frequency.

All the samples obtained by alternate current methods were observed by means of SEM to observe the morphology of the coatings at the different frequencies used. Fig. 9-a shows the micrograph of the coating obtained employing the 0.1 Hz frequency. As can be seen, the surface is coated with low size Pt nanoparticles finely dispersed on the RGO coating. When the frequency was increased to 1 Hz there was a significant increase in the degree of coating as well as the Pt nanoparticles size (Fig. 9-b). In this case, the Pt nanoparticles were covering the whole surface of the electrode. When the synthesis frequency was increased up to 10 Hz, the degree of coating increased again and the growth in the Z direction was also observed (Fig. 9-c). The nanoparticles size seemed to be similar to that obtained for 1 Hz. The samples obtained using 0.1, 1, and 10 Hz had identical synthesis time (55.6 s), so higher frequencies are most effective in the synthesis of Pt nanoparticles. The differences of electroactivity observed by means

of cyclic voltammetry can be attributed to a different degree of coating (Pt content) rather than the size of the nanoparticles. The other frequencies used had no comparable synthesis time since there was a limitation in the number of points, although similar morphologies of the coatings were obtained. The sample coated using the 100 Hz frequency showed similar morphology (Fig. 9-d) and even peeled off due to the massive growth of Pt nanoparticles (inset Fig. 9-d). The excessive growth of Pt coatings can lead to cracks on the surface of the coating [49]. Fig. 9-e shows a micrograph of an electrode obtained using the 1000 Hz synthesis frequency, a small size Pt nanoparticles dispersion can be observed. The low content of Pt nanoparticles can be correlated with the very low synthesis time (0.06 s). Similar results were observed for the 10000 Hz frequency (Fig. 9-f).

## 4. Conclusions

Reduced graphene oxide (RGO) has been synthesized on Pt electrodes by means of potentiodynamic technique; the most adequate lower potential limit to carry out the synthesis was -1.4 V (vs. Ag/AgCl 3.5 M KCl). X-ray photoelectron spectroscopy (XPS) results showed that electrochemical reduction method was more effective than the chemical reduction by sodium dithionite (used in our previous paper) as evidenced by the lower O/C ratio. The voltammetric characterization of Pt-RGO electrodes in 0.5 M $H_2SO_4$ solutions have shown the characteristic capacitative behavior of RGO. Once Pt-RGO electrodes were obtained, the synthesis of Pt nanoparticles (131.4 $\mu g \cdot cm^{-2}$) was carried out at different potentials (-0.16 V, 0 V, +0.2 V, +0.4 V) (vs. Ag/AgCl 3.5 M KCl) by means of potentiostatic synthesis. The electrodes obtained were characterized by means of cyclic voltammetry in 0.5 M $H_2SO_4$ solution to observe the characteristic

oxidation and reduction processes of the Pt surface. A 0.5 M $H_2SO_4$ / 0.5 M $CH_3OH$ solution was also used to measure the catalytic properties of the deposits against methanol oxidation. The results obtained have shown that the most adequate potentials to carry out the synthesis followed this order 0 V, -0.16 V, +0.2 V, +0.4 V (vs. Ag/AgCl 3.5 M KCl). The morphology of the coating was also greatly influenced by the potential used. At 0 V, a 2-D densely packed coating with very low grain size of Pt nanoparticles was obtained. At -0.16 V the formation of flower-like structures has been reported. At +0.2 V, dispersed Pt nanoparticles in the form of globules and with higher size were observed. Finally at +0.4 V, there was no substantial synthesis of Pt nanoparticles.

A new method for the synthesis of Pt nanoparticles on RGO coated electrodes was applied for the first time. The method consisted of the synthesis of Pt nanoparticles using alternate current obtained from electrochemical impedance spectroscopy equipment. Different frequencies were evaluated to find the best one; 0.1, 1, 10, 100, 1000 and 10000 Hz were used. In the impedance modulus $|Z|$ vs. the frequency (Hz) plot, the resistance of the electrodes decreased as the synthesis proceeded. With high frequencies it was not possible to obtain proper coatings since the synthesis time that could be obtained was very low due to the limitation in the number of points that could be acquired. The results for lower frequencies (0.1, 1, and 10 Hz) could be compared since the synthesis time employed was the same (55.6 s). The best results were obtained for 10 Hz followed by 1 Hz and 0.1 Hz. As observed by scanning electron microscopy (SEM), in this case the variation of the electrocatalytic properties seems to be related to the quantity of Pt deposited. Higher frequencies seem to be more effective in the synthesis of Pt nanoparticles than lower ones. The electrocatalytic properties, evaluated from the cyclic voltammetry response in different media, showed that electrodes obtained at the best synthesis frequency (10 Hz) had higher electroactivity (double) than

electrodes obtained by means of potentiostatic synthesis at 0 V (vs. Ag/AgCl 3.5 M KCl). The synthesis of Pt nanoparticles by alternate current methods has been shown to be of interest since less synthesis time is needed to obtain more electroactive coatings.

**Acknowledgements**

Authors wish to thank to the Spanish Ministerio de Ciencia e Innovación (contract CTM2011-23583) and Universitat Politècnica de València (Vicerrectorado de Investigación PAID-06-10 contract 003-233) for the financial support. J. Molina is grateful to the Conselleria d'Educació, Formació i Ocupació (Generalitat Valenciana) for the Programa VALi+D Postdoctoral Fellowship. A.I. del Río is grateful to the Spanish Ministerio de Ciencia y Tecnología for the FPI fellowship.

**Author contributions**

J. Molina performed the synthesis of the materials and wrote the paper. J. Fernández and A.I. del Río performed the CV characterization of the electrodes obtained. J. Bonastre performed the XPS measurements, the analysis of data and wrote this part of the paper. F. Cases designed the experiments and wrote the paper. All authors have approved the final article.

**References**

[1] Novoselov KS, Geim AK, Morozov SV, Jiang D, Zhang Y, Dubonos SV et al. Electric field effect in atomically thin carbon films. Science 2004;306:666–9.

[2] Geim AK, Novoselov KS. The rise of graphene. Nat Mat 2007;6:183–91.

[3] Geim AK. Graphene: status and prospects. Science 2009;324:1530–4.

[4] Castro Neto AH, Guinea F, Peres NMR, Novoselov KS, Geim AK. The electronic properties of graphene. Rev Modern Phys 2009;81:109–62.

[5] Heersche HB, Jarillo-Herrero P, Oostinga JB, Vandersypen LMK, Morpurgo AF. Bipolar supercurrent in graphene. Nature 2007;446:56–9.

[6] Allen MJ, Tung VC, Kaner RB. Honeycomb carbon: A review of graphene. Chem Rev 2010;110:132–45.

[7] Soldano C, Mahmood A, Dujardin E. Production, properties and potential of graphene. Carbon 2010;48:2127–50.

[8] Singh V, Joung D, Zhai L, Das S, Khondaker SI, Seal S. Graphene based materials: Past, present and future. Prog Mater Sci 2011;56:1178–271.

[9] Park S, Ruoff RS. Chemical methods for the production of graphenes. Nat Nanotechnol 2009;4:217–24.

[10] Zhou T, Chen F, Tang C, Bai H, Zhang Q, Deng H et al. The preparation of high performance and conductive poly (vinyl alcohol)/graphene nanocomposite via reducing graphite oxide with sodium hydrosulfite. Compos Sci Technol 2011;71:1266–70.

[11] Chen L, Tang Y, Wang K, Liu C, Luo S. Direct electrodeposition of reduced graphene oxide on glassy carbon electrode and its electrochemical application. Electrochem Commun 2011;13:133–7.

[12] Devadas B, Rajkumar M, Chen S-M, Saraswathi R. Electrochemically reduced graphene oxide/ neodymium hexacyanoferrate modified electrodes for the electrochemical detection of paracetomol. Int J Electrochem Sci 2012;7:3339–49.

[13] Hilder M, Winther-Jensen B, Li D, Forsyth M, MacFarlane DR. Direct electro-deposition of graphene from aqueous suspensions. Phys Chem Chem Phys 2011;13:9187–93.

[14] Zhou M, Wang Y, Zhai Y, Zhai J, Ren W, Wang F et al. Controlled synthesis of large-area and patterned electrochemically reduced graphene oxide films. Chem Eur J 2009;15:6116–20.

[15] Bonanni A, Pumera M. Electroactivity of graphene oxide on different substrates. R Soc Chem Adv 2012;2:10575–8.

[16] Guo S-X, Zhao S-F, Bond AM, Zhang J. Simplifying the evaluation of graphene modified electrode performance using rotating disk electrode voltammetry. Langmuir 2012;28:5275–85.

[17] Sheng K, Sun Y, Li C, Yuan W, Shi G. Ultrahigh-rate supercapacitors based on eletrochemically reduced graphene oxide for ac line-filtering. Sci Rep 2012;2:247.

[18] Huang H, Chen H, Sun D, Wang X. Graphene nanoplate-Pt composite as a high performance electrocatalyst for direct methanol fuel cells. J Power Sources 2012;204:46–52.

[19] Li Y, Gao W, Ci L, Wang C, Ajayan PM. Catalytic performance of Pt nanoparticles on reduced graphene oxide for methanol electro-oxidation. Carbon 2010;48:1124–30.

[20] Yoo E, Okata T, Akita T, Kohyama M, Nakamura J, Honma I. Enhanced electrocatalytic activity of Pt subnanoclusters on graphene nanosheet surface. Nano Lett 2009;9:2255–9.

[21] Park S, Shao Y, Wan H, Rieke PC, Viswanathan VV, Towne SA et al. Design of graphene sheets-supported Pt catalyst layer in PEM fuel cells. Electrochem Commun 2011;13:258–61.

[22] Li Y, Tang L, Li J. Preparation and electrochemical performance for methanol oxidation of Pt/graphene nanocomposites. Electrochem Commun 2009;11:846–9.

[23] He D, Cheng K, Li H, Peng T, Xu F, Mu S et al. Highly active platinum nanoparticles on graphene nanosheets with a significant improvement in stability and CO tolerance. Langmuir 2012;28:3979–86.

[24] Qiu J-D, Wang G-C, Liang R-P, Xia X-H, Yu H-W. Controllable deposition of platinum nanoparticles on graphene as an electrocatalyst for direct methanol fuel cells. J Phys Chem C 2011;115:15639–45.

[25] Chartarrayawadee W, Moulton SE, Li D, Too CO, Wallace GG. Novel composite graphene/platinum electro-catalytic electrodes prepared by electrophoretic deposition from colloidal solutions. Electrochim Acta 2012;60:213–23.

[26] Zhang Y, Liu C, Min Y, Qi X, Ben X. The simple preparation of graphene/Pt nanoparticles composites and their electrochemical performance. J Mater Sci: Mater Electron 2013;24:3244–8.

[27] Hsieh SH, Hsu MC, Liu WL, Chen WJ. Study of Pt catalyst on graphene and its application to fuel cell. Appl Surf Sci 2013;277:223–30.

[28] Dao V-D, Ho NTQ, Larina LL, Lee J-K, Choi H-S. Graphene–platinum nanohybrid as a robust and low–cost counter electrode for dye–sensitized solar cells. Nanoscale in press.

[29] Yeh M-H, Lin L-Y, Su J-S, Leu Y-A, Vittal R, Sun C-L et al. Nanocomposite graphene/Pt electrocatalyst as economical counter electrode for dye-sensitized solar cells. ChemElectroChem 0000, 00, 1–11. DOI: 10.1002/celc.201300081.

[30] Shafiei M, Spizzirri PG, Arsat R, Yu J, du Plessis J, Dubin S et al. Platinum/graphene nanosheet/SiC contacts and their application for hydrogen gas sensing. J Phys Chem C 2010;114:13796–801

[31] Chen X, Cai Z, Huang Z, Oyama M, Jiang Y, Chen X. Non-enzymatic oxalic acid sensor using platinum nanoparticles modified on graphene nanosheets. Nanoscale 2013;5:5779–83.

[32] Yin Z, He Q, Huang X, Zhang J, Wu S, Chen P et al. Real-time DNA detection using Pt nanoparticle-decorated reduced graphene oxide field-effect transistors. Nanoscale 2012;4:293–7.

[33] Wang H, Du J, Yao Z, Yue R, Zhai C, Jiang F et al. Facile fabrication, characterization of Pt–Ru nanoparticles modified reduced graphene oxide and its high electrocatalytic activity for methanol electro-oxidation. Colloid Surfaces A 2013;436:57–61.

[34] Gao L, Yue W, Tao S, Fan L. Novel strategy for preparation of graphene-Pd, Pt composite, and its enhanced electrocatalytic activity for alcohol oxidation. Langmuir 2013;29:957–64.

[35] Hilder M, Winther-Jensen O, Winther-Jensen B, MacFarlane DR. Graphene/zinc nano-composites by electrochemical co-deposition. Phys Chem Chem Phys 2012;14:14034–40.

[36] Lupu S, Lakard B, Hihn J-Y, Dejeu J. Novel in situ electrochemical deposition of platinum nanoparticles by sinusoidal voltages on conducting polymer films. Synthetic Met 2012;162:193−8.

[37] Clavilier J. The role of anion on the electrochemical behaviour of a {1 1 1} platinum surface; an unusual splitting of the voltammogram in the hydrogen region. J Electroanal Chem 1979;107:211−6.

[38] Zhang J, Ting BP, Khan M, Pearce MC, Yang Y, Gao Z et al. Pt nanoparticle label-mediated deposition of Pt catalyst for ultrasensitive electrochemical immunosensors. Biosens Bioelectron 2010;26:418−23.

[39] Wang J. Analytical Electrochemistry. 2nd. New York: Wiley-VCH; 2000.

[40] Kim CS, Oh SM. Enzime sensors prepared by electrodeposition on platinized platinum electrodes. Electrochim Acta 1996;41:2433–9.

[41] Qiang L, Vaddiraju S, Rusling JF, Papadimitrakopoulos F. Highly sensitive and reusable Pt-black microfluidic electrodes for long-term electrochemical sensing. Biosens Bioelectron 2010;26:682–8.

[42] Kicela A, Daniele S. Platinum black coated microdisk electrodes for the determination of high concentrations of hydrogen peroxide in phosphate buffer solutions. Talanta 2006;68:1632–9.

[43] Stankovich S, Dikin DA, Dommett GHB, Kohlhaas KM, Zimney EJ, Stach EA et al. Graphene-based composite materials. Nature 2006;440:282–6.

[44] Wagner CD, Naumkin AV, Kraut-Vass A, Allison JW, Powell CJ, Rumble Jr JR. NIST X-ray photoelectron spectroscopy database, The National Institute of Standards and Technology, U.S. Department of Commerce, 2007, Available from: http://srdata.nist.gov/xps/Default.aspx (last accessed 20.11.13).

[45] Benoit R, Durand Y, Narjoux B, Quintana G. X-ray photoelectron spectroscopy database. La Surface, CNRS and Thermo Fisher Scientific, Thermo Electron France. Available from: http://www.lasurface.com/database/elementxps.php. (last accessed 20.11.13).

[46] Yang D, Velamakanni A, Bozoklu G, Park S, Stoller M, Piner RD et al. Field DA, Ventrice Jr CA, Ruoff RS. Chemical analysis of graphene oxide films after heat and chemical treatments by X-ray photoelectron and micro-Raman spectroscopy. Carbon 2009;47:145–52.

[47] Kormunda M, Pavlik J. Characterization of oxygen and argon ion flux interaction with PET surfaces by in-situ XPS and ex-situ FTIR. Polym Degrad Stabil 2010;95:1783–8.

[48] Molina J, Fernández J, del Río AI, Bonastre J, Cases F. Chemical and electrochemical study of fabrics coated with reduced graphene oxide. Appl Surf Sci 2013;279:46–54.

[49] Wei ZD, Chan SH, Li LL, Cai HF, Xia ZT, Sun CX. Electrodepositing Pt on a Nafion-bonded carbon electrode as a catalyzed electrode for oxygen reduction reaction. Electrochim Acta 2005;50:2279–87.

[50] Domínguez-Domínguez S, Arias-Pardilla J, Berenguer-Murcia A, Morallón E, Cazorla-Amorós D. Electrochemical deposition of platinum nanoparticles on different carbon supports and conducting polymers. J Appl Electrochem 2008;38:259–68.

[51] Molina J, Fernández J, del Río AI, Bonastre J, Cases F. Characterization of azo dyes on Pt and Pt/polyaniline/dispersed Pt electrodes. Appl Surf Sci 2012;258:6246–56.

[52] Huang L-M, Tang W-R, Wen T-C. Spatially electrodeposited platinum in polyaniline doped with poly(styrene sulfonic acid) for methanol oxidation. J Power Sources 2007;164:519–26.

[53] Singh RN, Awasthi R, Tiwari SK. Electro-catalytic activities of binary nano-composites of Pt and nano- carbon/multiwall carbon nanotube for methanol electro-oxidation. Open Catal J 2010;3:50–7.

[54] Li G-R, Xu H, Lu X-F, Feng J-X, Tong Y-X, Su C-Y. Electrochemical synthesis of nanostructured materials for electrochemical energy conversion and storage. Nanoscale 2013;5:4056–69.

[55] Yao Z, Zhu M, Jiang F, Du Y, Wang C, Yang P. Highly efficient electrocatalytic performance based on Pt nanoflowers modified reduced graphene oxide/carbon cloth electrode. J Mater Chem 2012;22:13707−13.

**Figure captions**

Fig. 1. Cyclic voltammograms of RGO-Pt (20 scans of synthesis between +0.6 V and -1.4 V) and Pt in 0.5 M $H_2SO_4$ solution. Scan potential range: from -0.2 V to +0.7 V. Scan rate: 50 $mV \cdot s^{-1}$. First scan shown for all the measurements. Potentials referred to Ag/AgCl 3.5 M KCl reference electrode.

Fig. 2. FESEM micrographs of Pt-RGO electrode: a) (x 5.77 K), b) (x 25.8 K).

Fig. 3. a) High resolution C 1s XPS core level spectrum for RGO sample; (b) High resolution O 1s XPS core level spectrum for Pt-RGO sample.

Fig. 4. Cyclic voltammograms of RGO-Pt (obtained after 20 scans of synthesis between +0.6 V and -1.4 V) in 0.5 M $H_2SO_4$ solution and 0.5 M $H_2SO_4$ / 5 mM $H_2PtCl_6$ solutions. Potentials referred to Ag/AgCl 3.5 M KCl reference electrode.

Fig. 5. Cyclic voltammograms of Pt-RGO-Pt electrodes. Pt coatings synthesized at different potentials (-0.16 V, 0 V, 0.2 V and 0.4 V) and with the same electrical charge of 260 $mC \cdot cm^{-2}$. a) 0.5 M $H_2SO_4$, second scan for all samples b) 0.5 M $H_2SO_4$ / 0.5 M

methanol, fifth scan for all samples. Scan potential range: between -0.2 V and +1.0 V; scan rate, 50 $mV \cdot s^{-1}$. Potentials referred to Ag/AgCl 3.5 M KCl reference electrode.

Fig. 6. FESEM micrographs of Pt-RGO-Pt electrodes synthesized at different potentials and with the same electrical charge of 260 $mC \cdot cm^{-2}$: a) -0.16 V (x 20.1 K), b) -0.16 V (x 210.22 K), c) 0 V (x 20.1 K), d) 0 V (x 243.72 K), e) +0.2 V (x 20.1 K), f) +0.2 V (x 206.37 K). Potentials referred to Ag/AgCl 3.5 M KCl reference electrode.

Fig. 7. Impedance modulus $|Z|$ vs. frequency (Hz) plot for the synthesis of Pt employing alternate current synthesis method on RGO-Pt electrodes (synthesized potentiodinamically between +0.6 V and -1.4 V for 20 scans). Synthesis of Pt performed in 0.5 M $H_2SO_4$ / 5 mM $H_2PtCl_6$ solutions. Potential set at +0.4 V (potential at which the synthesis of Pt is not produced), perturbation potential applied to produce the synthesis ±350 mV. a) Synthesis performed at different frequencies (0.1 Hz, 1 Hz, 10 Hz, 100 Hz, 1000 Hz, 10000 Hz). Pt was also deposited employing the $10^5$-$10^{-2}$ Hz frequency range for comparison employing ±10 mV and ±350 mV perturbation waves. b) Magnified plot that shows the data for the synthesis performed with the 10 Hz frequency range. Potentials referred to Ag/AgCl 3.5 M KCl reference electrode.

Fig. 8. Cyclic voltammograms of Pt-RGO-Pt electrodes. Coating of Pt synthesized by alternate current methods at different frequencies (0.1 Hz, 1 Hz, 10 Hz, 100 Hz, 1000 Hz, 10000 Hz). Pt was also deposited on another electrode employing the $10^5$-$10^{-2}$ Hz frequency range for comparison (same conditions). One sample was also synthesized at +0.4 V during 6000 s to discard the synthesis of Pt at this potential. a) 0.5 M $H_2SO_4$, second scan for all samples b) 0.5 M $H_2SO_4$ / 0.5 M methanol, fifth scan for all samples.

Scan potential range: from -0.2 V to +1.0 V; scan rate, 50 $mV \cdot s^{-1}$. Potentials referred to Ag/AgCl 3.5 M KCl reference electrode.

Fig. 9. FESEM micrographs of Pt-RGO-Pt electrodes synthesized by alternate current methods at different frequencies. a) 0.1 Hz (x 50.18 K), b) 1 Hz (x 50.18 K), c) 10 Hz (x 50.18 K), d) 100 Hz (x 2.04 K), e) 1000 Hz (x 50.18 K), f) 10000 Hz (x 50.18 K).

**Table captions**

Table 1. Parameters employed for the synthesis and parameters obtained for the characterization of the Pt-RGO-Pt electrodes obtained by potentiostatic synthesis.

Table 2. Parameters employed for the synthesis and parameters obtained for the characterization of the Pt-RGO-Pt electrodes obtained by alternate current methods.

**Table(1)**

Table 1. Parameters employed for the synthesis and parameters obtained for the characterization of the Pt-RGO-Pt electrodes obtained by potentiostatic synthesis.

| Synthesis potential (V) | Synthesis charge ($mC \cdot cm^{-2}$) | Pt loading ($\mu g \cdot cm^{-2}$) | Morphology | Hydrogen adsorption charge ($mC \cdot cm^{-2}$)[(1)] | ECSA ($m^2/g$)[(2)] | Roughness factor[(3)] | $j_{+0.65V}$ ($mA \cdot cm^{-2}$)[(4)] | $j_{+0.45V}$ ($mA \cdot cm^{-2}$)[(5)] |
|---|---|---|---|---|---|---|---|---|
| -0.16 | 260 | 131.4 | Flower-like structure | 6.74 | 24.42 | 32.09 | 23.14 | 17.87 |
| 0 | 260 | 131.4 | Flat continuous coating | 8.36 | 30.30 | 39.82 | 32.97 | 27.74 |
| +0.2 | 260 | 131.4 | Globular | 3.84 | 13.92 | 18.29 | 6.31 | 4.86 |
| +0.4 | 260 | No synthesis observed | - | - | - | - | - | - |

Common parameters: electrode material (Pt-RGO synthesized during 20 scans by CV between +0.6 V and -1.4 V), synthesis solution (0.5 M $H_2SO_4$ / 5 mM $H_2PtCl_6$), counter electrode (Pt), reference electrode (Ag/AgCl 3.5 M), characterizing solutions (0.5 M $H_2SO_4$ and 0.5 M $H_2SO_4$ / 0.5 M $CH_3OH$).

[(1)]Calculated with the integration of the hydrogen adsorption area in the voltammogram obtained in 0.5 M $H_2SO_4$ [19].

[(2)] Calculated dividing the hydrogen adsorption charge by the Pt loading and the theoretical value for the adsorption of a hydrogen monolayer on Pt surface (210 $\mu C \cdot cm^{-2}$) [19].

[(3)]Calculated dividing the normalized hydrogen adsorption charge ($\mu C \cdot cm^{-2}$) by the theoretical value for the adsorption of a hydrogen monolayer on Pt surface (210 $\mu C \cdot cm^{-2}$) [41].

[(4)]Maximum current density observed in the voltammograms obtained in 0.5 M $H_2SO_4$ / 0.5 M $CH_3OH$ solution at +0.65 V.

[(5)]Maximum current density observed in the voltammograms obtained in 0.5 M $H_2SO_4$ / 0.5 M $CH_3OH$ solution at +0.45 V.

**Table(2)**

Table 2. Parameters employed for the synthesis and parameters obtained for the characterization of the Pt-RGO-Pt electrodes obtained by alternate current methods.

| | Frequency (Hz) | | | | | | | | | |
|---|---|---|---|---|---|---|---|---|---|---|
| Nomenclature | High | Low | Points | Synthesis time (s) | Real synthesis time (s) | Morphology | Hydrogen adsorption charge ($mC \cdot cm^{-2}$)[(1)] | Roughness factor[(2)] | $j_{+0.65V}$ ($mA \cdot cm^{-2}$)[(3)] | $j_{+0.45V}$ ($mA \cdot cm^{-2}$)[(4)] |
| $10^5$-$10^{-2}$ Hz | 100000 | 0.01 | 50 | 357 | 178.5 | Globular | 6.30 | 29.99 | 15.56 | 12.20 |
| 0.1 Hz | 0.1 | 0.08 | 10 | 111 | 55.6 | Globular | 2.06 | 9.82 | 2.96 | 2.37 |
| 1 Hz | 1 | 0.8 | 100 | 111 | 55.6 | Globular | 7.89 | 37.55 | 16.72 | 15.27 |
| 10 Hz | 10 | 8 | 1000 | 111 | 55.6 | Globular | 19.99 | 95.20 | 58.55 | 50.27 |
| 100 Hz | 100 | 80 | 1000 | 11.1 | 5.56 | Globular | 20.94 | 99.69 | 36.88 | 22.10 |
| 1000 Hz | 1000 | 800 | 100 | 0.111 | 0.0556 | Globular | 1.63 | 7.75 | 0.29 | 0.09 |
| 10000 Hz | 10000 | 8000 | 1000 | 0.111 | 0.0556 | Globular | 1.42 | 6.77 | 0.19 | 0.04 |

Common parameters: electrode material (Pt-RGO synthesized during 20 scans by CV between +0.6 V and -1.4 V), synthesis solution (0.5 M $H_2SO_4$ / 5 mM $H_2PtCl_6$), counter electrode (Pt), reference electrode (Ag/AgCl 3.5 M), characterizing solutions (0.5 M $H_2SO_4$ and 0.5 M $H_2SO_4$ / 0.5 M $CH_3OH$).

[(1)]Calculated with the integration of the hydrogen adsorption area in the voltammogram obtained in 0.5 M $H_2SO_4$ [19].

[(2)]Calculated dividing the normalized hydrogen adsorption charge ($\mu C \cdot cm^{-2}$ by the theoretical value for the adsorption of a hydrogen monolayer on Pt surface (210 $\mu C \cdot cm^{-2}$) [41].

[(3)]Maximum current density observed in the voltammograms obtained in 0.5 M $H_2SO_4$ / 0.5 M $CH_3OH$ solution at +0.65 V.

[(4)]Maximum current density observed in the voltammograms obtained in 0.5 M $H_2SO_4$ / 0.5 M $CH_3OH$ solution at +0.45 V.

**High-resolution Figure(1)**

**Click here to download high resolution image**

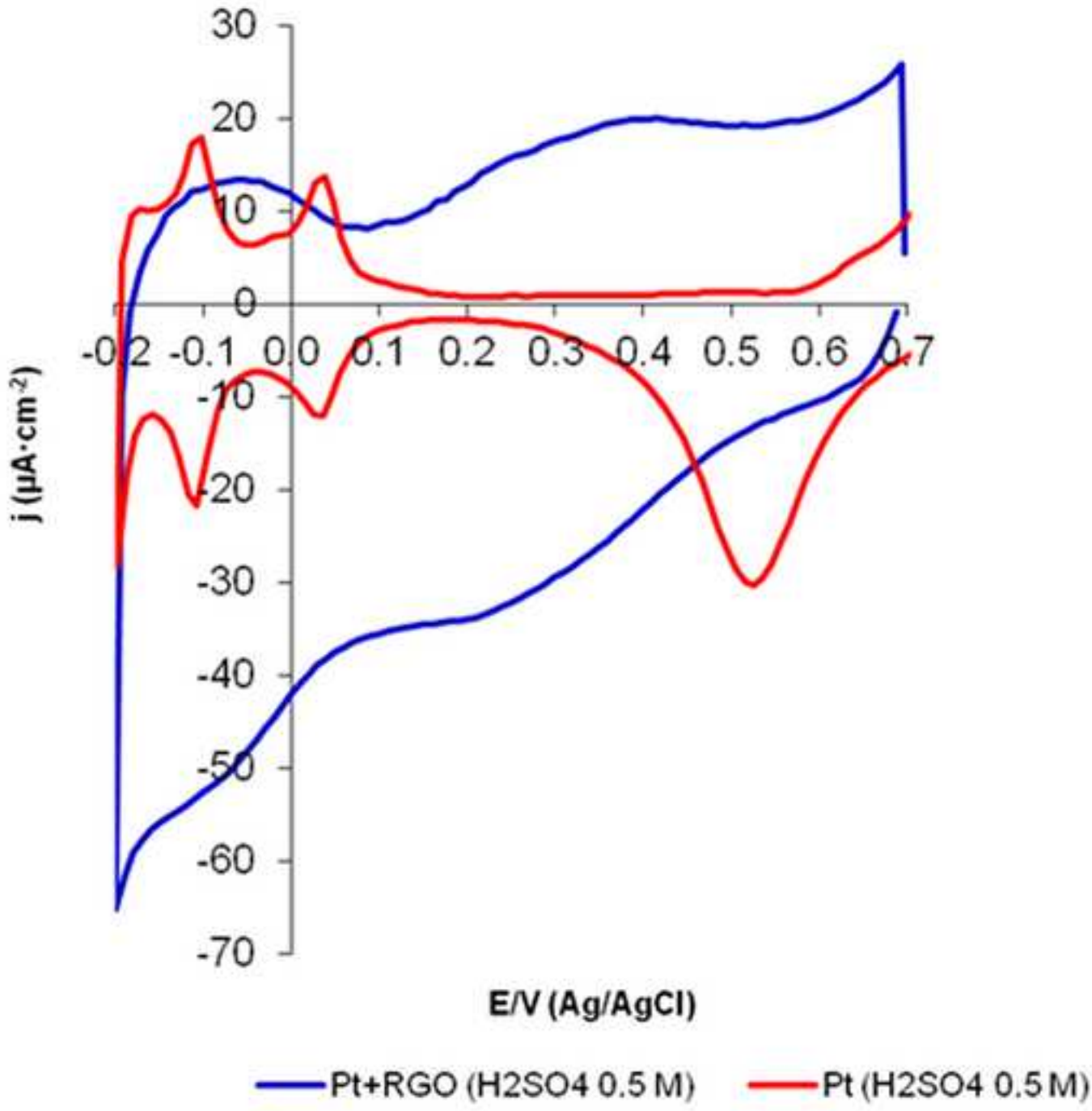

**High-resolution Figure(2)**

**Click here to download high resolution image**

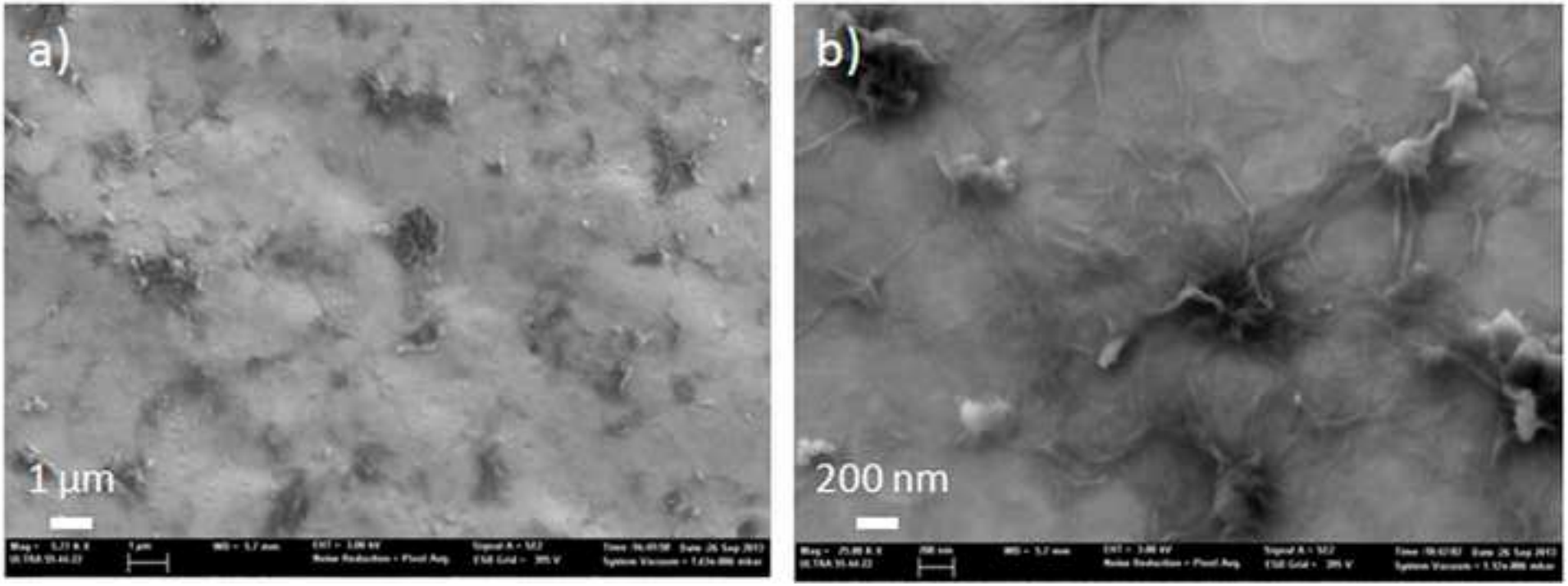

**High-resolution Figure(3)**
**Click here to download high resolution image**

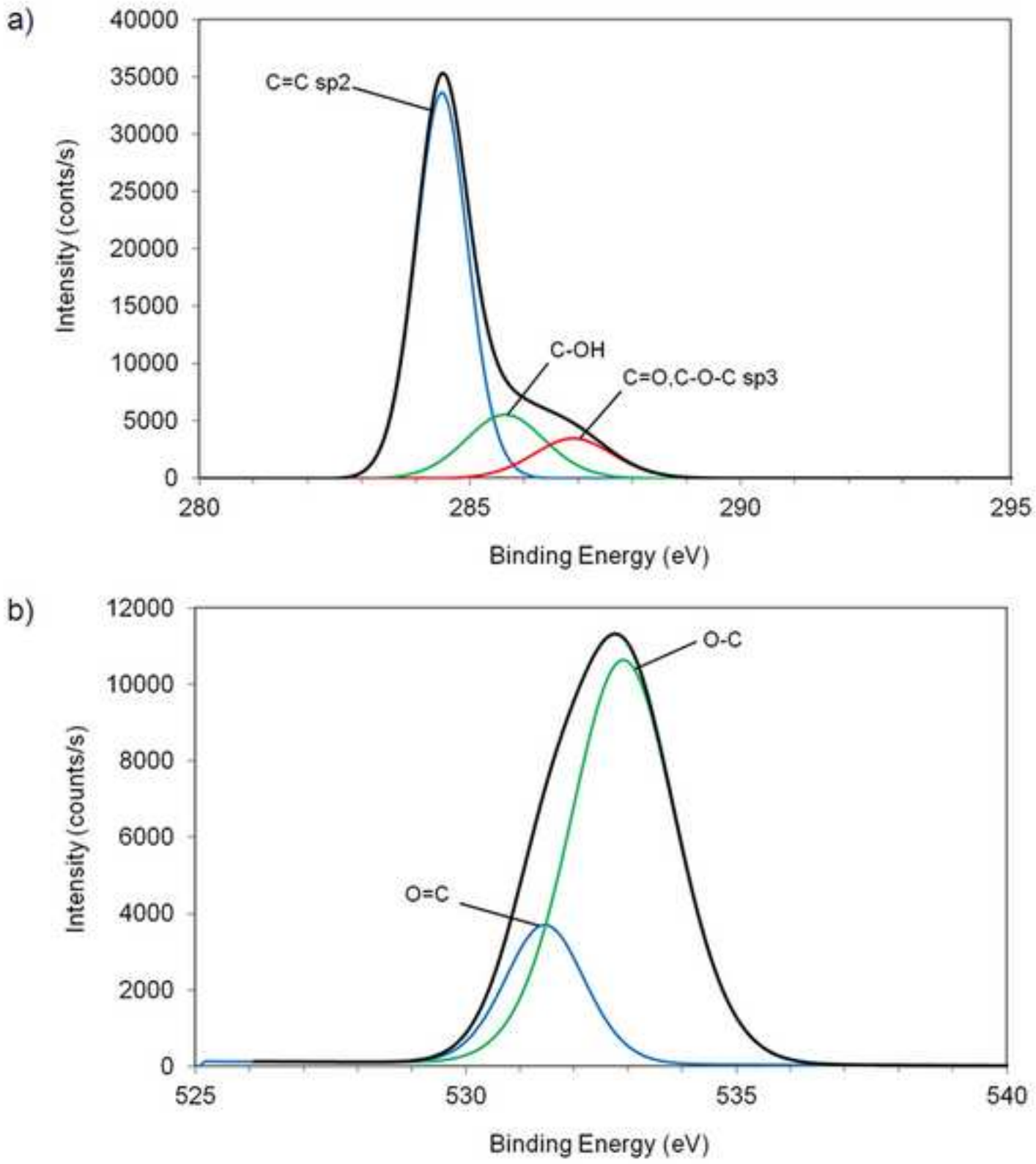

**High-resolution Figure(4)**

**Click here to download high resolution image**

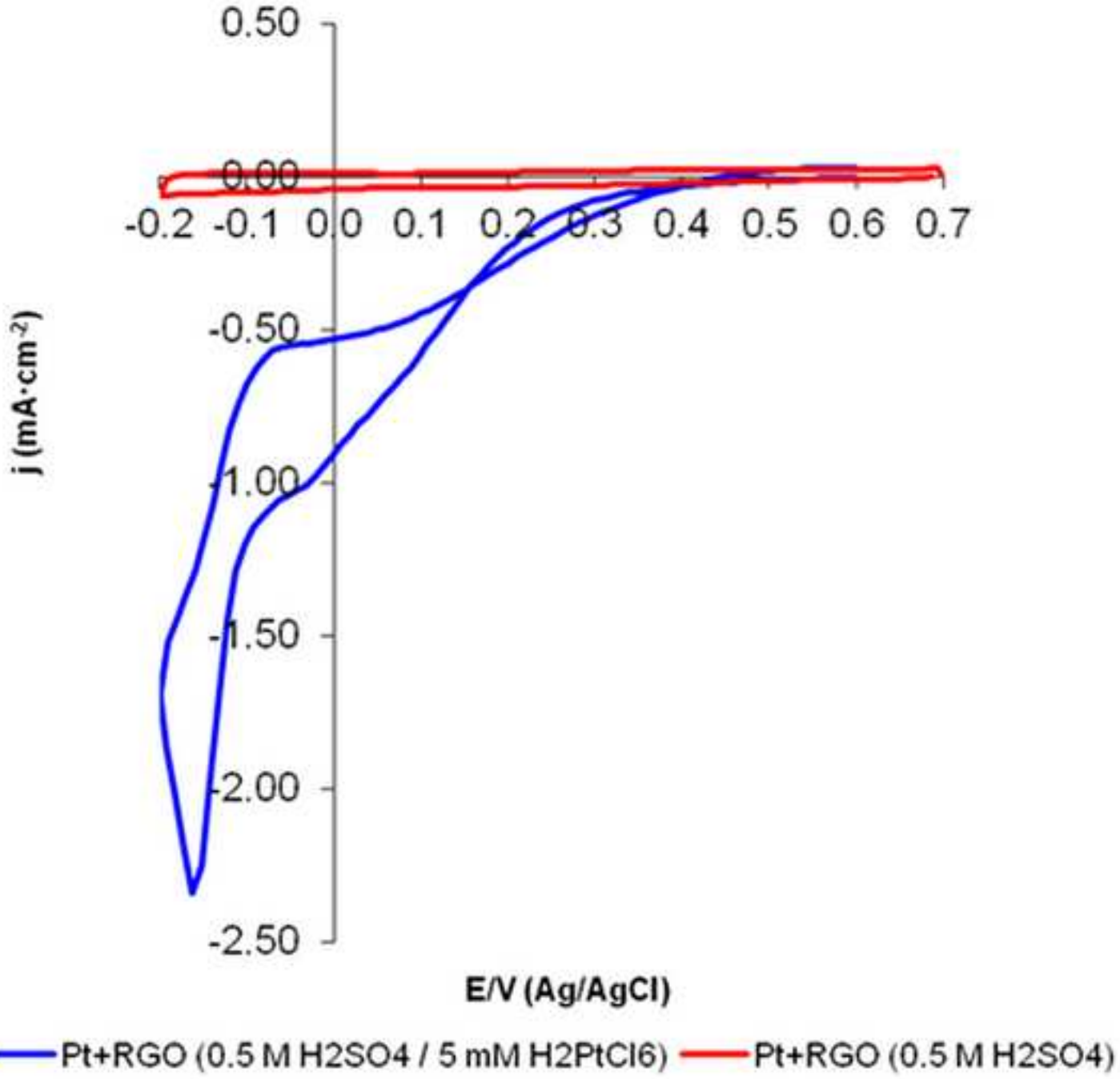

**High-resolution Figure(5)**
**Click here to download high resolution image**

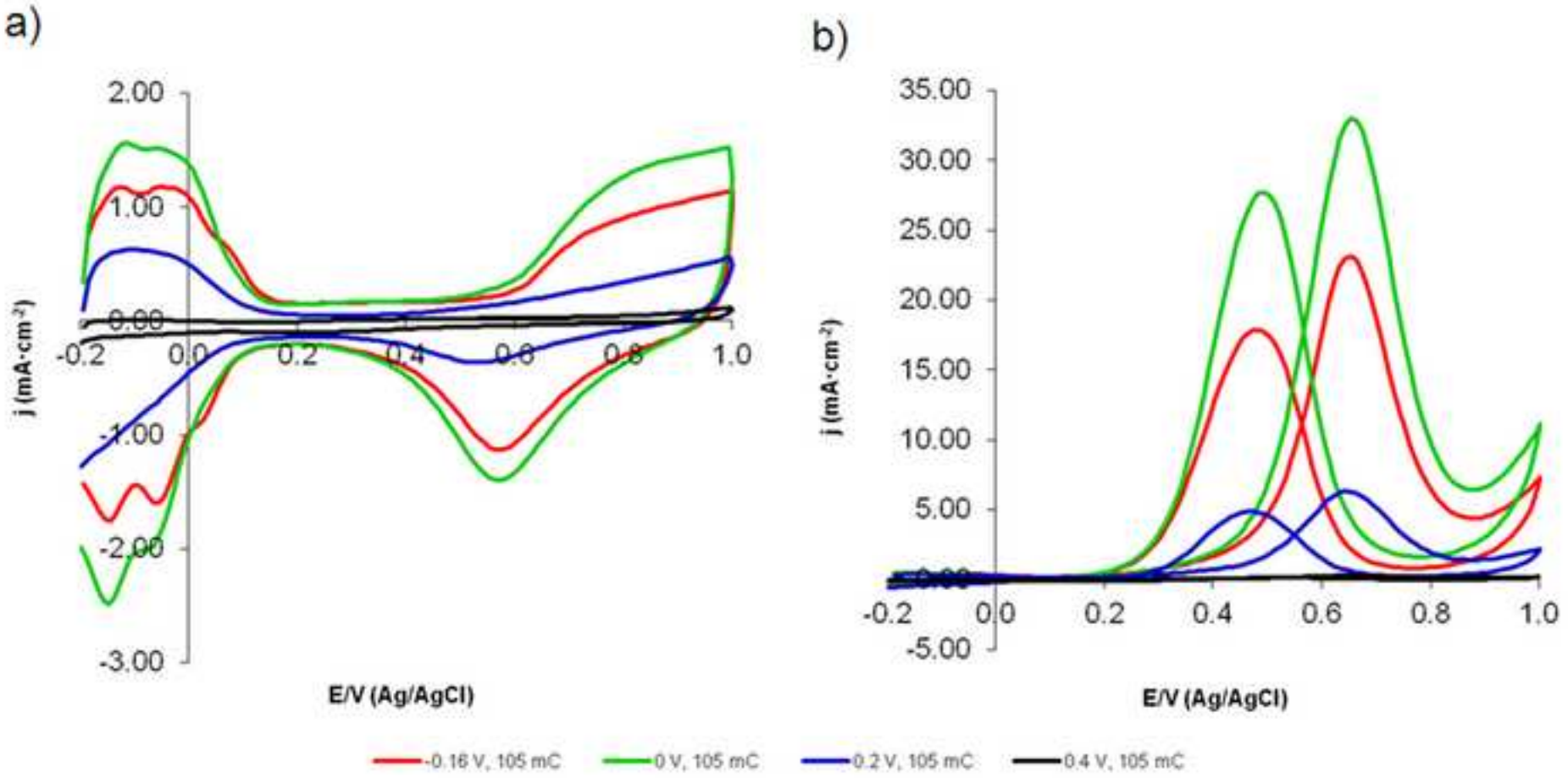

High-resolution Figure(6)
Click here to download high resolution image

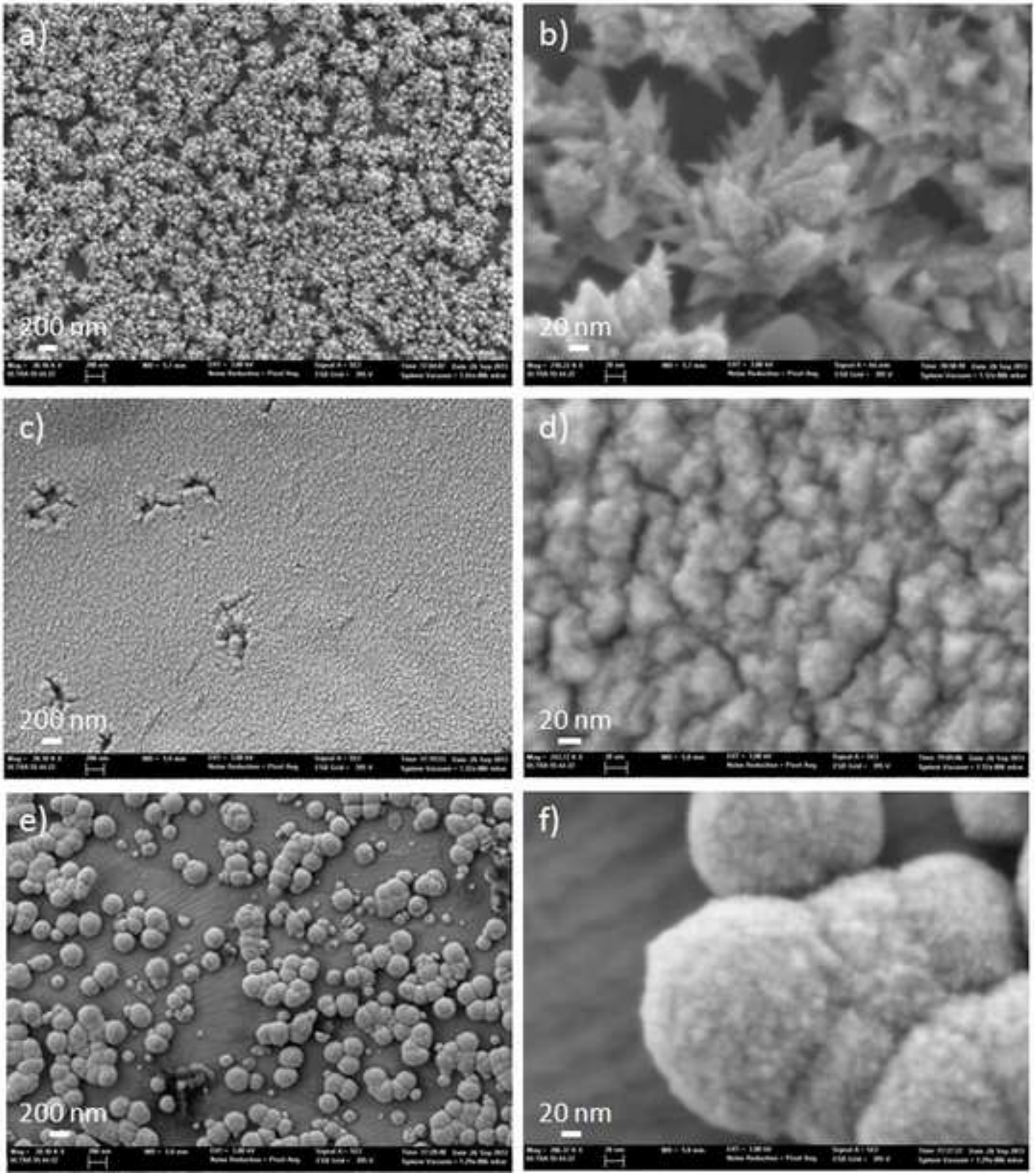

**High-resolution Figure(7)**

**Click here to download high resolution image**

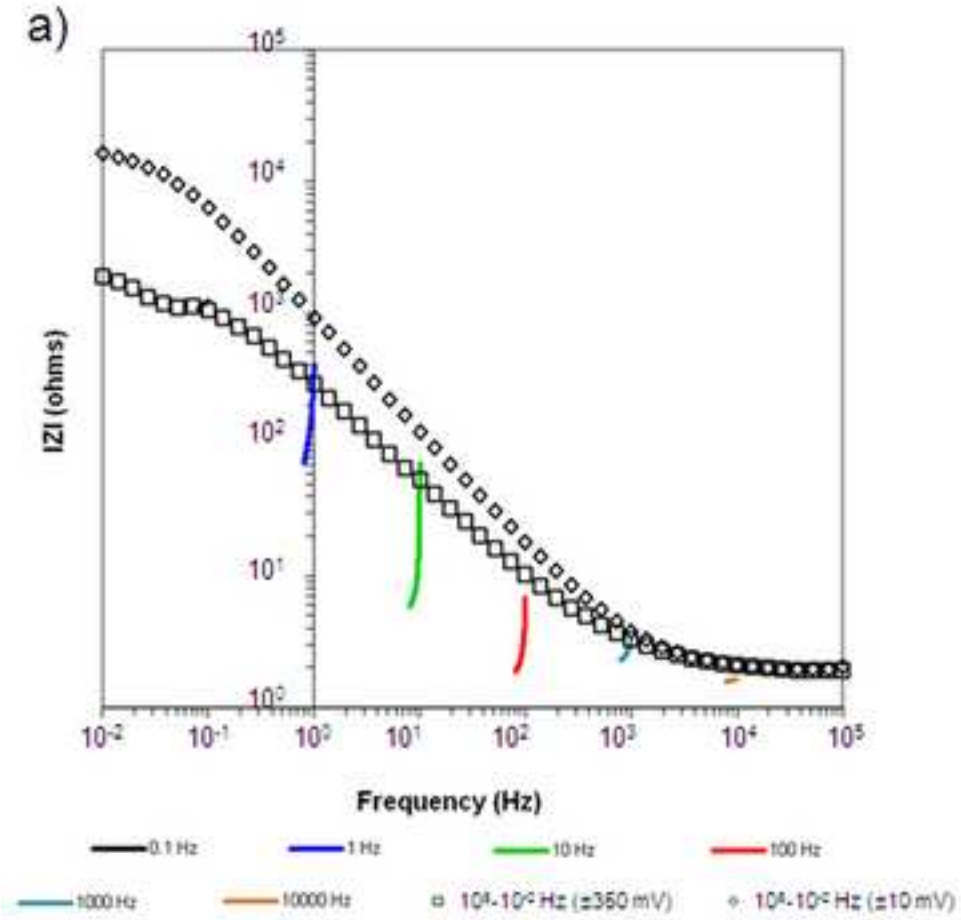


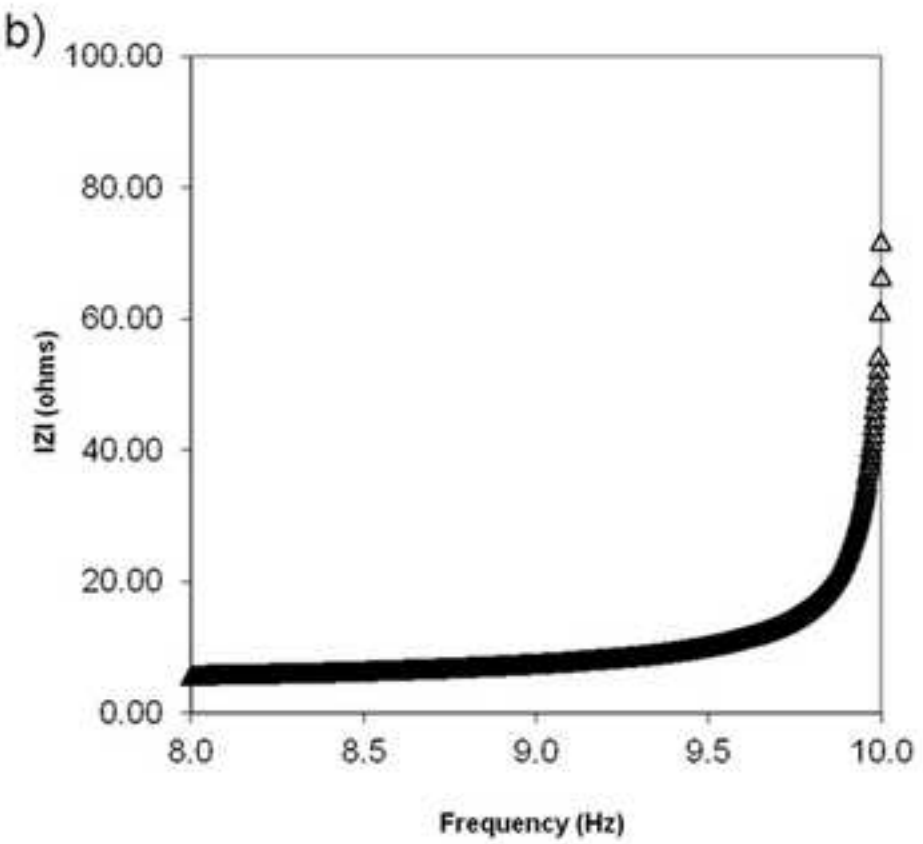

**High-resolution Figure(8)**

**Click here to download high resolution image**

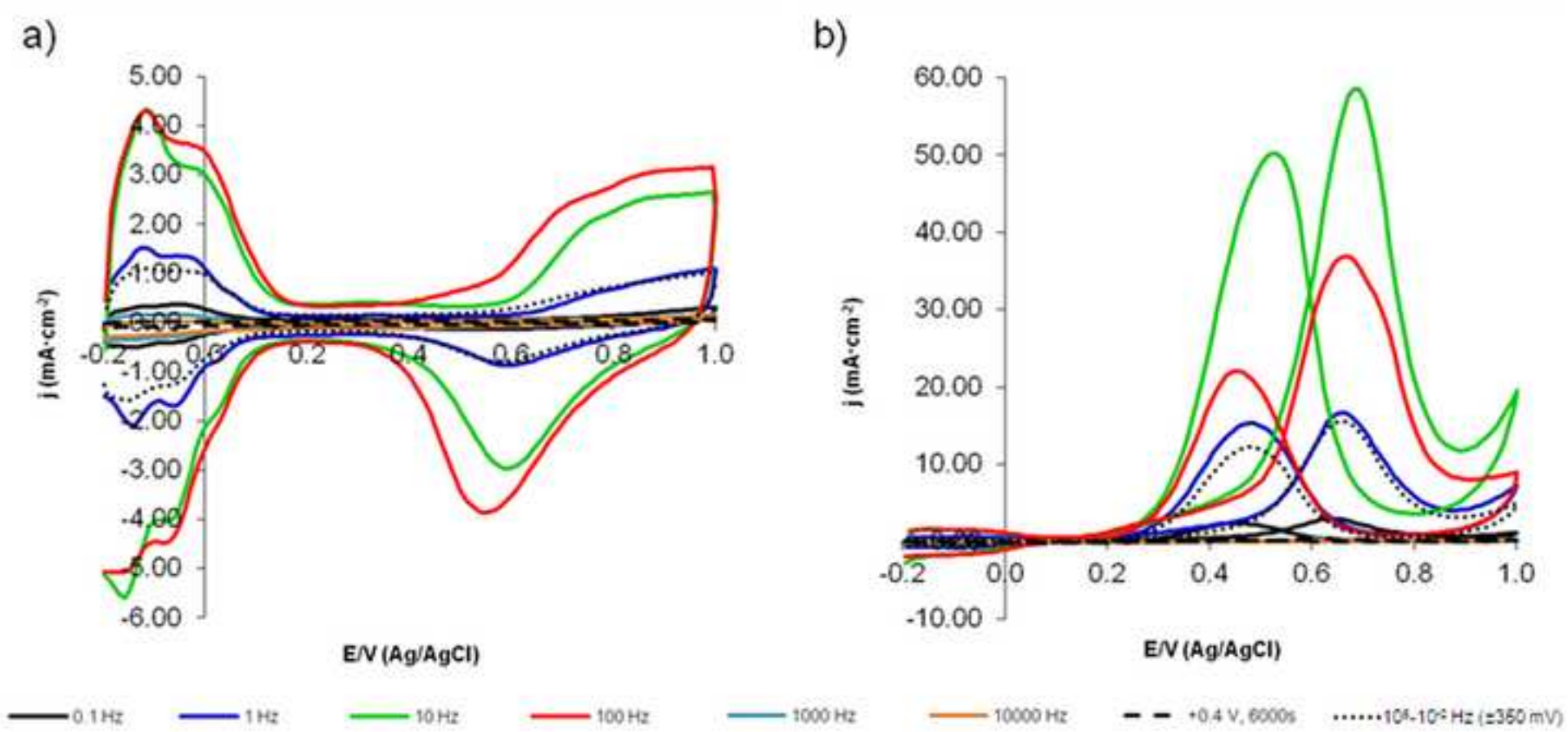

**High-resolution Figure(9)**

**Click here to download high resolution image**

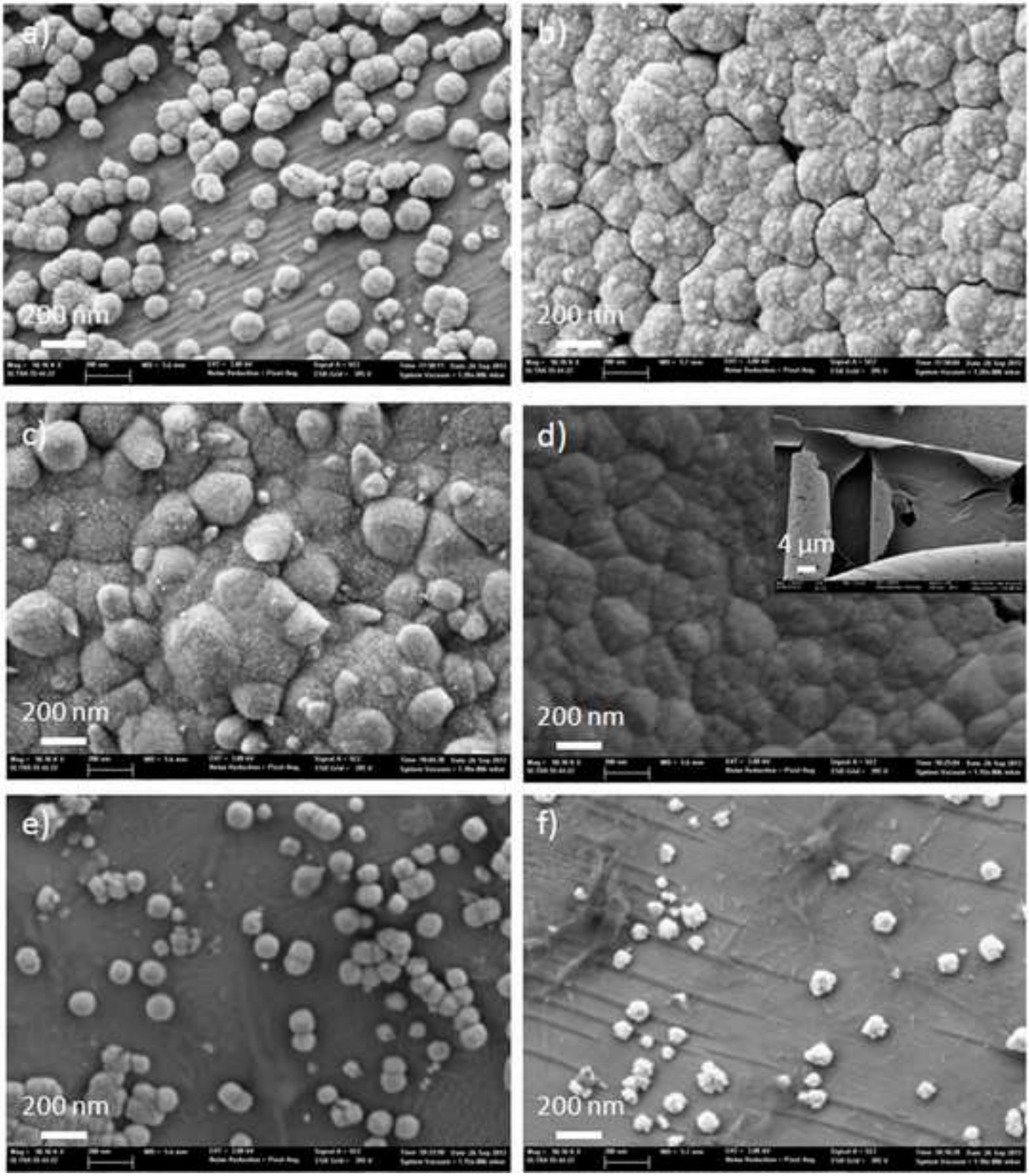

**Supplementary Material, Figure S1**
**Click here to download high resolution image**

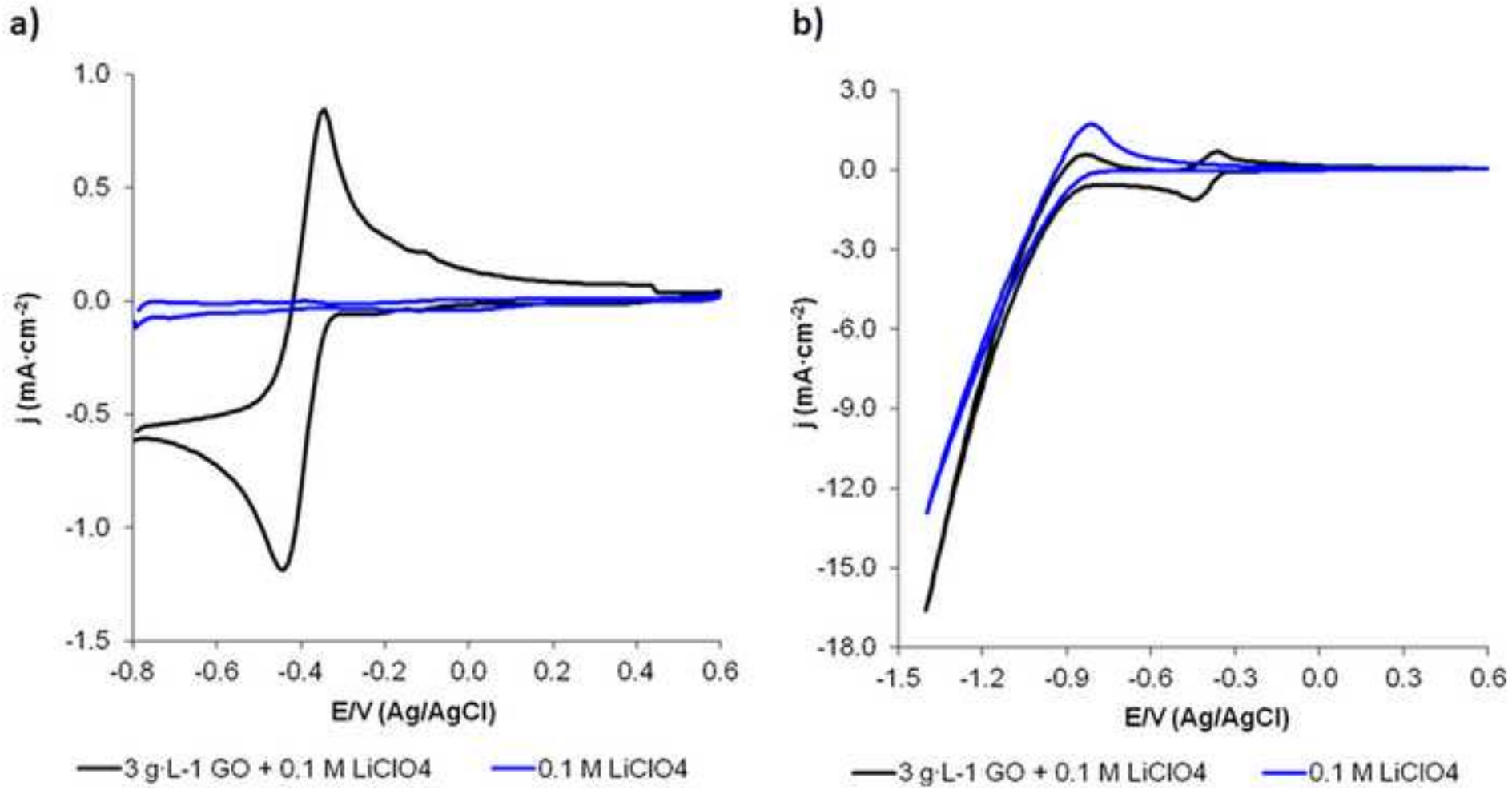

**Supplementary Material, Figure S2**

**Click here to download high resolution image**

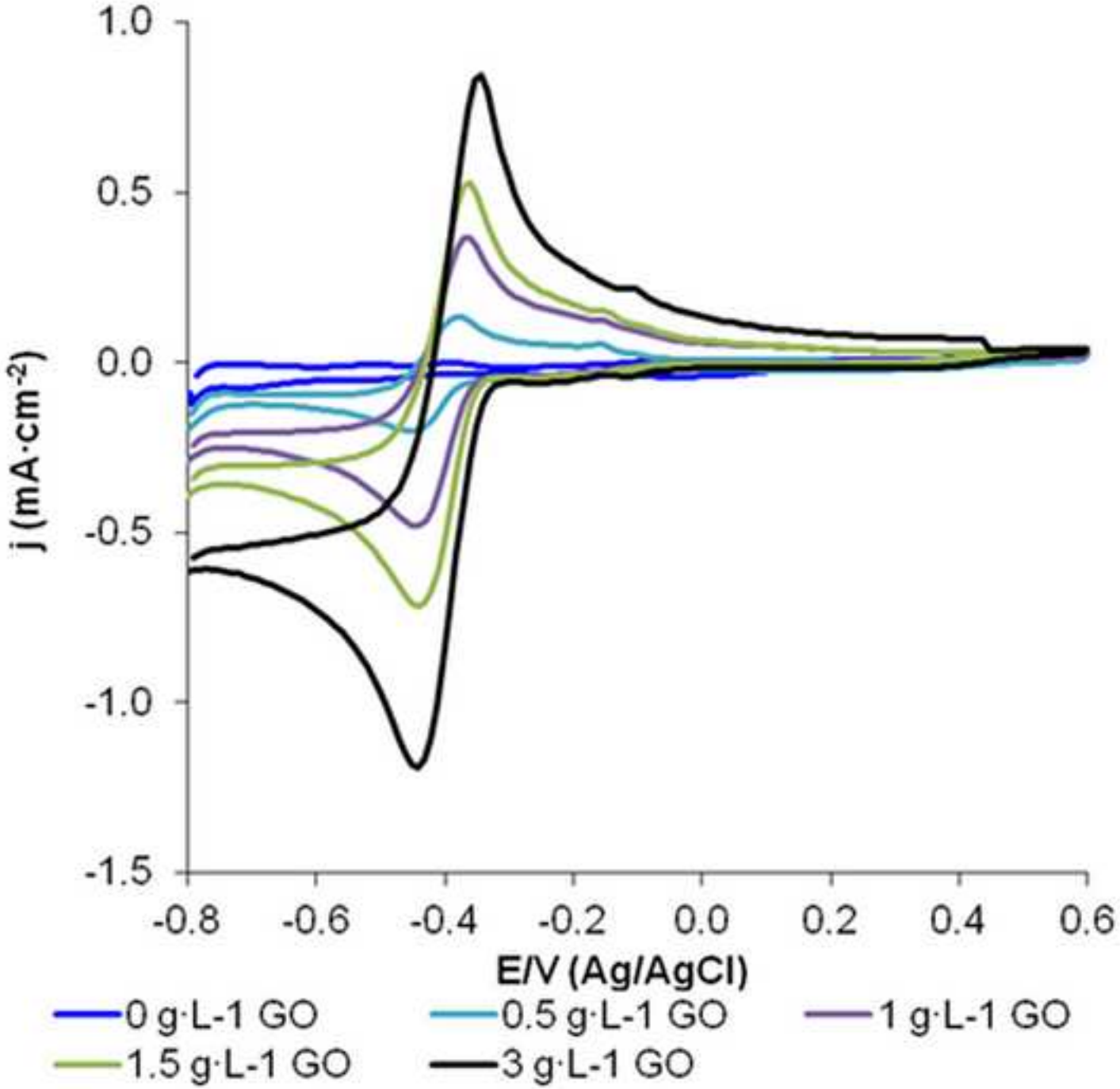

**Supplementary Material, Figure S3**
**Click here to download high resolution image**

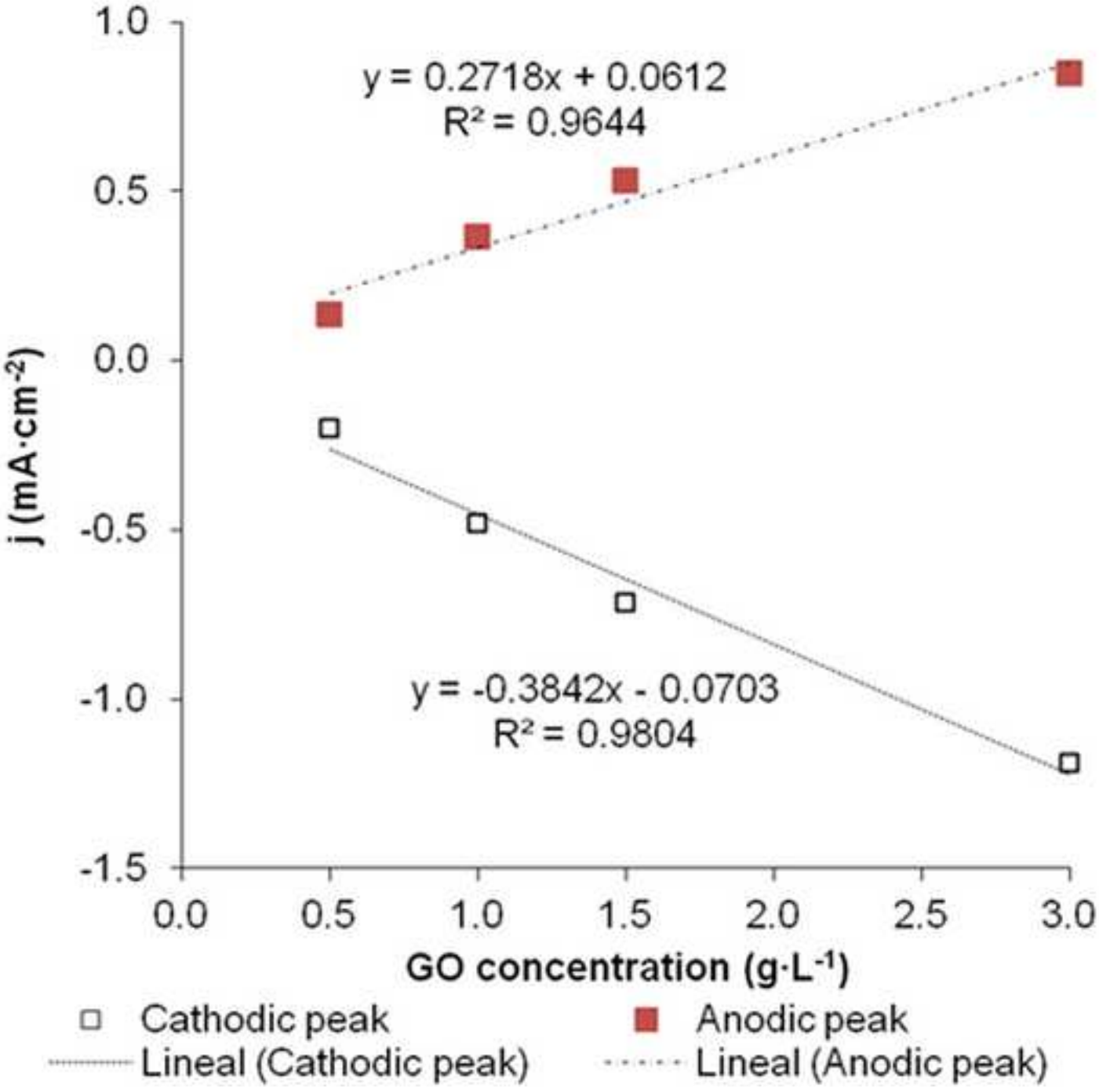

**Supplementary Material, Figure S4**

**Click here to download high resolution image**

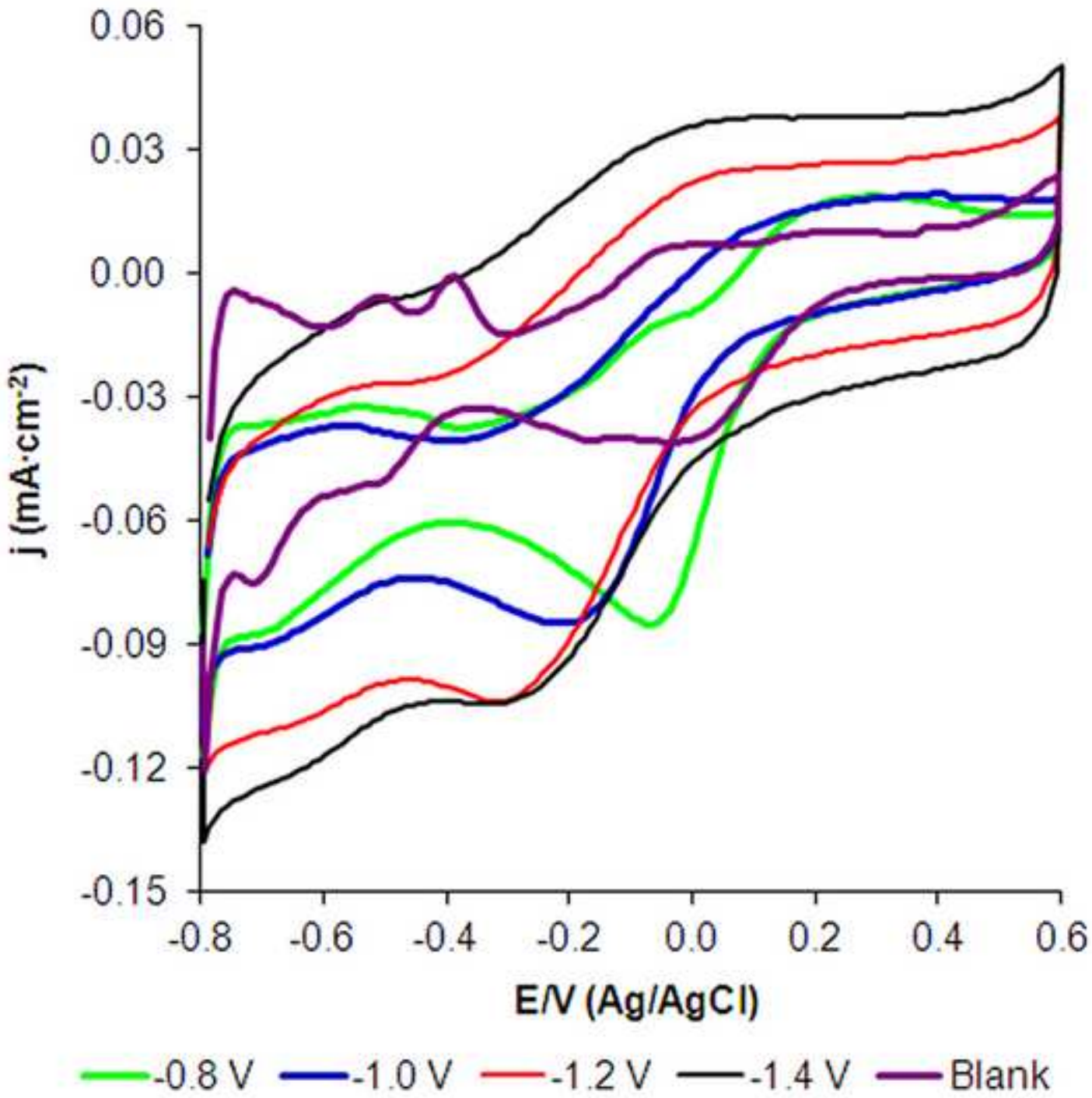

**Supplementary Material, Figure S5**

**Click here to download high resolution image**

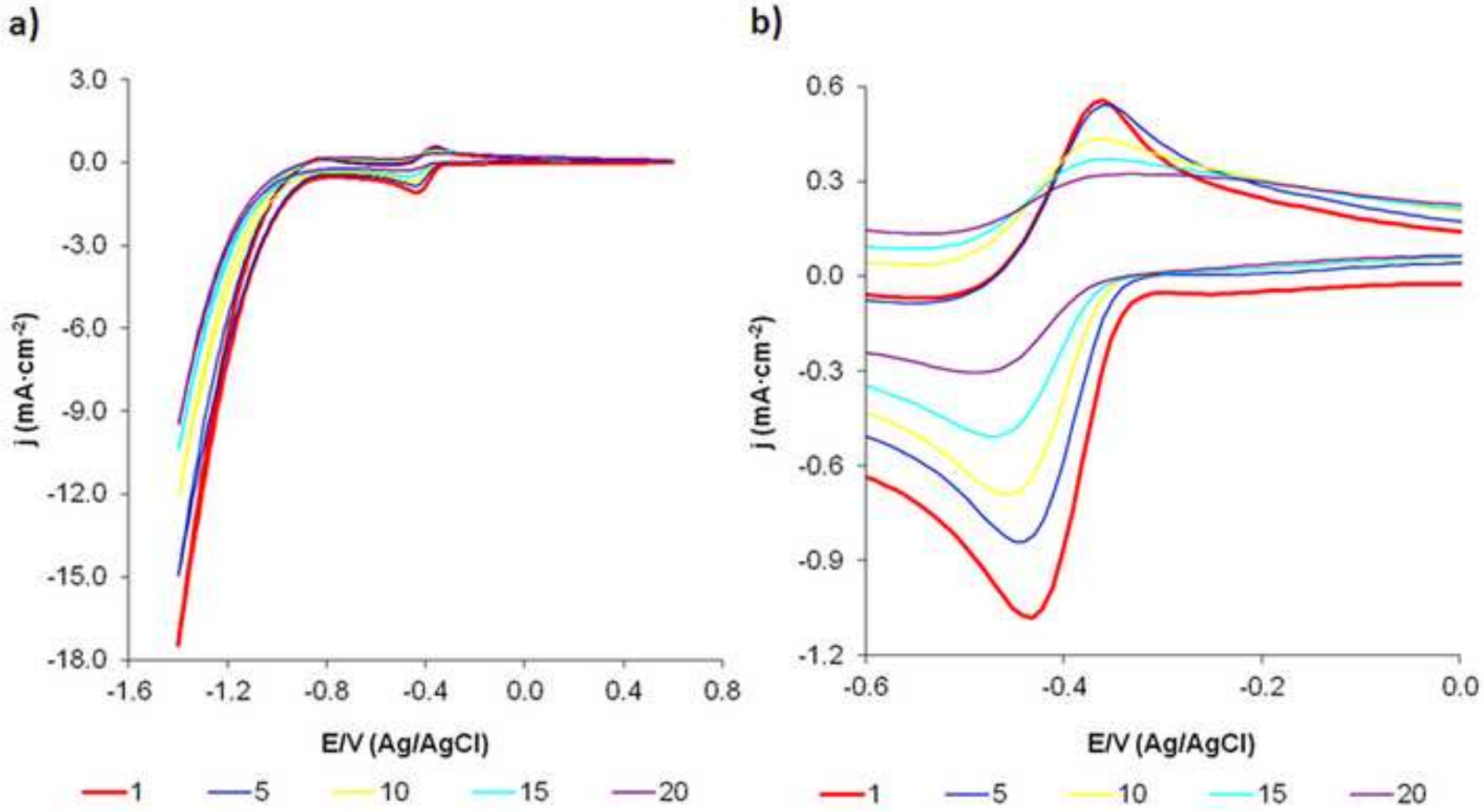

**Supplementary Material, Figure S6**
**Click here to download high resolution image**

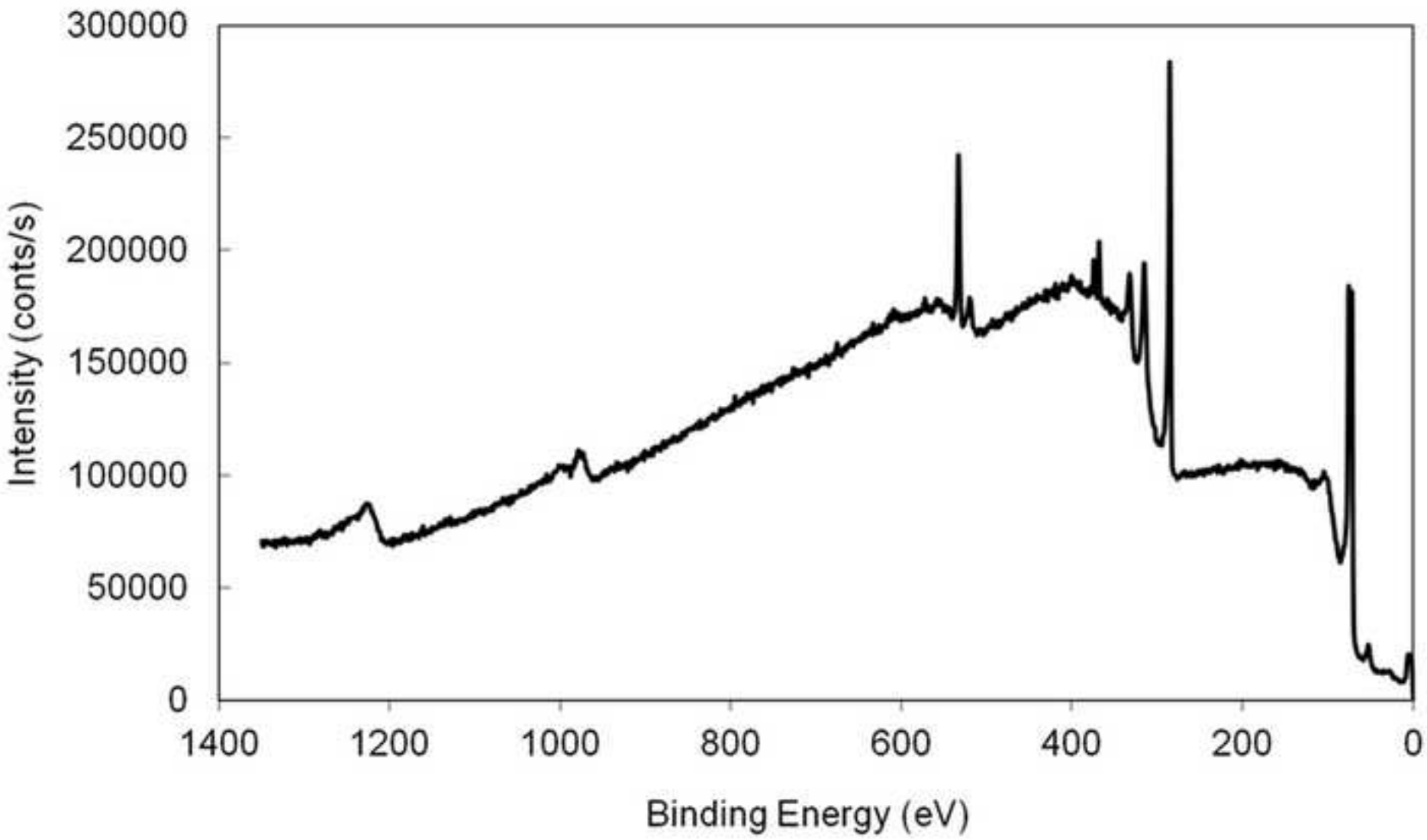

**Supplementary Material, Figure S7**
**Click here to download high resolution image**